

Supporting Information for

On the Scale of Heterogeneity in Composite Electrodes of Batteries

Aishwary Shrivastava^{1†}, Nikhil Sharma^{1†}, Xiaomei He^{1†}, Yijin Liu², Kejie Zhao^{1*}

¹School of Mechanical Engineering, Purdue University; West Lafayette, IN 47907, USA.

²Walker Department of Mechanical Engineering, The University of Texas at Austin; Austin, TX 78705, USA.

[†]These authors contributed equally to this work

*Corresponding author. Email: kjzhao@purdue.edu

This PDF file includes:

Supporting text Figures S1 to S52 Legend for Movie S1 SI References

Other supporting materials for this manuscript include the following:

Movie S1

Supporting Information Text Experimental details

The commercial NMC 532 cathode coated on 14 μ m aluminum substrate with a coating density of 10.8 mg cm⁻² and a total thickness of 60 μ m was first cut into 13 mm discs. The electrode was mounted on a glass slide using a very thin layer of epoxy and gently pressed using the broad end of a plastic pipette. The cathode needs to be flat on the glass slide for better polishing results. The sample was transferred to the rotary stage of the broad beam ion polisher (JEOL IB-19500CP Cross Section Polisher). The glass slide is mounted on the rotary stage platform using double-sided copper tape. The midpoint of ion flux is kept around 50 μ m from the top surface of the sample. The chamber is vacuumed, and Argon gas begins to flow through the chamber.

Three process parameters are tuned: Argon gas flow rate, orientation and location of the sample about the ion beam center, and the voltage across the top and bottom surfaces. The ion current bombarding the sample surface can be optimized by tuning three parameter values. An appropriate Ar flow rate is necessary to sweep the ion polish area and increase the material removal rate. Too high argon flow drastically reduces the net current density, and too little Ar flow creates a rough polishing surface. Various polishing experiments are performed to tune the sample's location and orientation from the beam center.

High voltage is necessary to create material removal in brittle ceramic materials like NMC. A voltage value of 6-6.5V is used. The XRD analysis is performed further to measure the structural information of the surface, and SEM images are used to tune the ion polishing process parameters. The rotary stage provides an option to rotate the sample while the ion beam current falls near the surface of the cathode. The polishing time was kept between 15-30 minutes.

Theory for the optical properties

The optical properties of solids are given by the response of the electronic structure to the electromagnetic perturbation caused by incoming light, which is calculated based on the independent-particle approximation (i.e., neglecting the local-field effects) in DFT. Such properties can be fully described using a complex dielectric function, $\varepsilon(\omega) = \varepsilon_1(\omega) + i\varepsilon_2(\omega)$, where $\varepsilon_1(\omega)$ and $\varepsilon_2(\omega)$ represent the real and imaginary parts of the dielectric function at all photon-frequencies ω , respectively. Optical quantities, such as reflectivity, absorption coefficient, and refraction index, can be obtained from $\varepsilon_1(\omega)$ and $\varepsilon_2(\omega)$. The imaginary part of the dielectric function due to electronic transitions is given by Fermi golden rule (1-3),

$$\varepsilon_2(\omega) = \frac{4\pi^2 e^2}{\Omega m^2 \omega^2} \sum_{c,v,\mathbf{k}} |\langle \mathbf{k} n^c | \mathbf{p} | \mathbf{k} n^v \rangle|^2 \delta(E_{\mathbf{k}n}^c - E_{\mathbf{k}n}^v - \hbar \omega), \tag{1}$$

where e is the electron charge, m is the effective mass of electron, and Ω is the cell volume. The momentum operator \mathbf{p} is obtained from the self-consistent band structures within the PAW formalism implemented by Furthmüller (4), $|\mathbf{k}n\rangle$ is the wave function corresponding to the n^{th} eigenvalue $E_{\mathbf{k}n}$ with the crystal wave vector \mathbf{k} , c(v) is conduction (valence) band states, \hbar represents the reduced Planck constant, and δ is Dirac's delta function which represents the energy conservation relationship of the transition process. The real part $\varepsilon_1(\omega)$ is obtained from $\varepsilon_2(\omega)$ using the Kramer-Kronig transformation (5),

$$\varepsilon_1(\omega) = 1 + \frac{2}{\pi} \mathbf{p} \int_0^\infty \frac{\varepsilon_2(\omega')\omega'}{\omega'^2 - \omega^2} d\omega'. \tag{2}$$

The Kramer-Kronig equation, derived from Cauchy integral, provides a means to obtain the real part if the imaginary part of the system is known at all frequencies $\omega'(0\to\infty)$. The refraction index $n(\omega)$ and the extinction coefficient $k(\omega)$ can be obtained from $\varepsilon_1(\omega)$ and $\varepsilon_2(\omega)$ given by

$$n(\omega) = \frac{1}{\sqrt{2}} \left[\sqrt{\varepsilon_1^2(\omega) + \varepsilon_2^2(\omega)} + \varepsilon_1(\omega) \right]^{\frac{1}{2}}, \tag{3}$$

$$k(\omega) = \frac{1}{\sqrt{2}} \left[\sqrt{\varepsilon_1^2(\omega) + \varepsilon_2^2(\omega)} - \varepsilon_1(\omega) \right]^{\frac{1}{2}}.$$
 (4)

The optical reflectivity $R(\omega)$ and absorption coefficient $\alpha(\omega)$ are

$$R(\omega) = \frac{[n(\omega)-1]^2 + k^2(\omega)}{[n(\omega)+1]^2 + k^2(\omega)'}$$
(5)

$$\alpha(\omega) = \frac{2\omega k(\omega)}{c} = \frac{\varepsilon_2(\omega)\omega}{n(\omega)c}.$$
 (6)

The obtained $\varepsilon_1(\omega)$ and $\varepsilon_2(\omega)$ spectra at different states-of-charge (SOCs) by GGA + D3 and GGA + U + D3 frameworks are shown in Fig. S12. The dashed vertical lines denote infrared, visible light, and ultraviolet regions. The in-plane ($E_{\parallel ab}$) and out-of-plane ($E_{\parallel c}$) polarization vectors show an anisotropic behavior at the photon energy ranging from infrared to ultraviolet. We note that Hubbard +U corrections shift the spectra slightly to a lower frequency, but the main feature remains. However, adding the U parameter increases the noise of the spectra, as shown in Fig. S12C and Fig. S12D. Therefore, we use GGA + D3 to investigate the optical responses of NMC.

Fig. S13 plots the static dielectric constants $\varepsilon_1(0)$ along $E_{\parallel ab}$ and $E_{\parallel c}$ as a function of the delithiation state as well as its average value ($[2\varepsilon_1^{ab}(0) + \varepsilon_1^{c}(0)]/3$). The average value of $\varepsilon_1(0)$ increases as Li composition decreases. According to the Penn model for semiconductors (6), $\varepsilon_1(0)\approx 1+(h\omega_p/E_g)^2$ where $\omega_p^2=4\pi Ne^2/m$ and $\varepsilon_1(0)$ is inversely related to the energy gap E_g of materials. Indeed, a lower energy gap often corresponds to higher electronic conductivity. Here the result indicates an increasing trend of electronic conductivity in NMC during Li extraction, which is consistent with literature reports (7, 8). Furthermore, comparing NMC532 and NMC811, $\varepsilon_1(0)$ shows a higher value with the higher content of Ni, which is also associated with a reduction in the band gap (9). As Ni

portion increases from NMC532 to NMC811, the increasing electron/hole carry density and more Ni at the higher oxidation states (Ni³⁺/Ni⁴⁺) both contribute to the enhanced electrical conductivity. It should be mentioned that due to the general band gap underestimation in PBE, an overestimation of $\epsilon_1(0)$ is expected.

The features of the real and imaginary parts of the complex dielectric constant are closely related to the electronic structure. Density of states (DOS) analysis of the pristine state (x = 0.0) and high delithiated state (x = 0.6) of NMC811 is shown in Fig. S14. A narrow peak (I) at 0.25 ± 0.1 eV in the infrared region and a broader peak (II) at 2.6 ± 0.1 eV within the Vis spectrum of imaginary part $\varepsilon_2(\omega)$ (Fig. S12B) can be understood as follows: Peak I can be assigned to electronic transitions in bands located closely to the Fermi level, such as TM-3d intraband transitions, given that both the valence band maximum (VBM) and the conduction band minimum (CBM) are dominated by TM-3d states. Likewise, peak II stems from TM-3d and O-2p interband transitions, encompassing the bands ranging roughly from 2.0 eV below the VBM to 0.5 eV above the CBM. The heightened value of peak II during delithiation correlates with the enhanced interband transitions as more occupation of O-2p states occurs at ~2.0 eV below the VBM and 0.5 eV above the CBM.

The absorption coefficient serves as a quantitative gauge of light absorption within a specific medium, which is directly associated with $\varepsilon_2(\omega)$. Within the Vis region, delithiation induces red shift of the optical absorption edge (Fig. S15). The absorption peaks in the Vis region are in line with the peaks obtained in $\varepsilon_2(\omega)$. The red-shift and increased absorption coefficient as Ni content increases from NMC532 to NMC811 can be attributed to the overall reduction of the energy gap (9, 10), as well as the stronger interband transitions (Fig. S14).

The refractive index describes propagation of an electromagnetic wave through a solid. It is closely related to the distribution of ions along the directions of polarization. Notably, the refractive index is sensitive to the delithiation state in the visible region; especially when light is polarized along the *ab*-plane (grey arrows), it results in significant growth of the refractive index during Li extraction (Fig. S16).

Governing equations for computational modeling

The Butler-Vomer equation represents the charge transfer kinetics at the interface between the active NMC and electrolyte. CB fully covers the surface of the NMC particles, and the rest of the NMC surface is exposed to the electrolyte. Li-ions transporting through the electrolyte meet the electrons traveling from the cathode current collector through the CB domain on the surface of the NMC particles. For the homogenized carbon binder domain, porosity is defined as ϵ_l and the carbon binder fraction is defined as ϵ_{CB} , $\epsilon_l + \epsilon_{CB} = 1$.

Using the Bruggeman relationship, the effective transport properties for the electrolyte within the porous carbon binder domain are

$$D_{l_{eff}} = \epsilon_l^{1.5} \cdot D_l, \tag{7}$$

$$K_{l\,eff} = \epsilon_l^{1.5} \cdot K_l, \tag{8}$$

$$K_{CB_eff} = \epsilon_l^{1.5} \cdot K_{CB}. \tag{9}$$

Li transport inside NMC particle follows Fick's diffusion law,

$$J_{NMC} = -D_{NMC} \nabla c_{NMC}, \tag{10}$$

$$\frac{\partial c_{NMC}}{\partial t} + \nabla \cdot J_{NMC} = 0, \tag{11}$$

where J_{NMC} is Li flux, D_{NMC} is Li diffusivity, and c_{NMC} is Li concentration. The Butler-Volmer equation describes charge transfer kinetics at the interface between the active particles and the electrolyte. The overpotential (η) is defined as:

$$\eta = \phi_s - \phi_l - E_{eq},\tag{12}$$

$$i_0 = F(k_C)^{\alpha_a} (k_a)^{\alpha_c} (c_{max} - c)^{\alpha_a} (c)^{\alpha_c} \left(\frac{c_l}{c_{lref}}\right)^{\alpha_a}, \tag{13}$$

$$i_{BV} = (\boldsymbol{pen}) * i_0 \left(\exp\left(\frac{\alpha_a F \eta}{RT}\right) - \exp\left(\frac{-\alpha_c F \eta}{RT}\right) \right).$$
 (14)

Here, *pen* is the penalty factor assigned randomly to all the particles and is fixed for each particle throughout the simulation. The value of *pen* varies between the values of 0 and 1 and follows Weibull distribution,

$$f(x;\lambda,k) = \begin{cases} \frac{k}{\lambda} \left(\frac{x}{\lambda}\right)^{k-1} e^{-(x/\lambda)^k}, & x \ge 0, \\ 0, & x < 0 \end{cases}$$
 (15)

The boundary conditions of charge transfer at the interface between the electrolyte and NMC are

$$i_l \cdot \mathbf{n} = -i_{BV}$$
, $i_S \cdot \mathbf{n} = i_{BV}$. (16)

The boundary conditions of mass conservation at the interface are given by

$$J_l \cdot \mathbf{n} = -\frac{i_{BV}}{F}, \qquad J_{NMC} \cdot \mathbf{n} = \frac{i_{BV}}{F}.$$
 (17)

where \mathbf{n} is the normal unit vector at the specified surfaces. The numerical values of the parameters in the modeling are identical to our previous work (Tables S2-4 in (11))

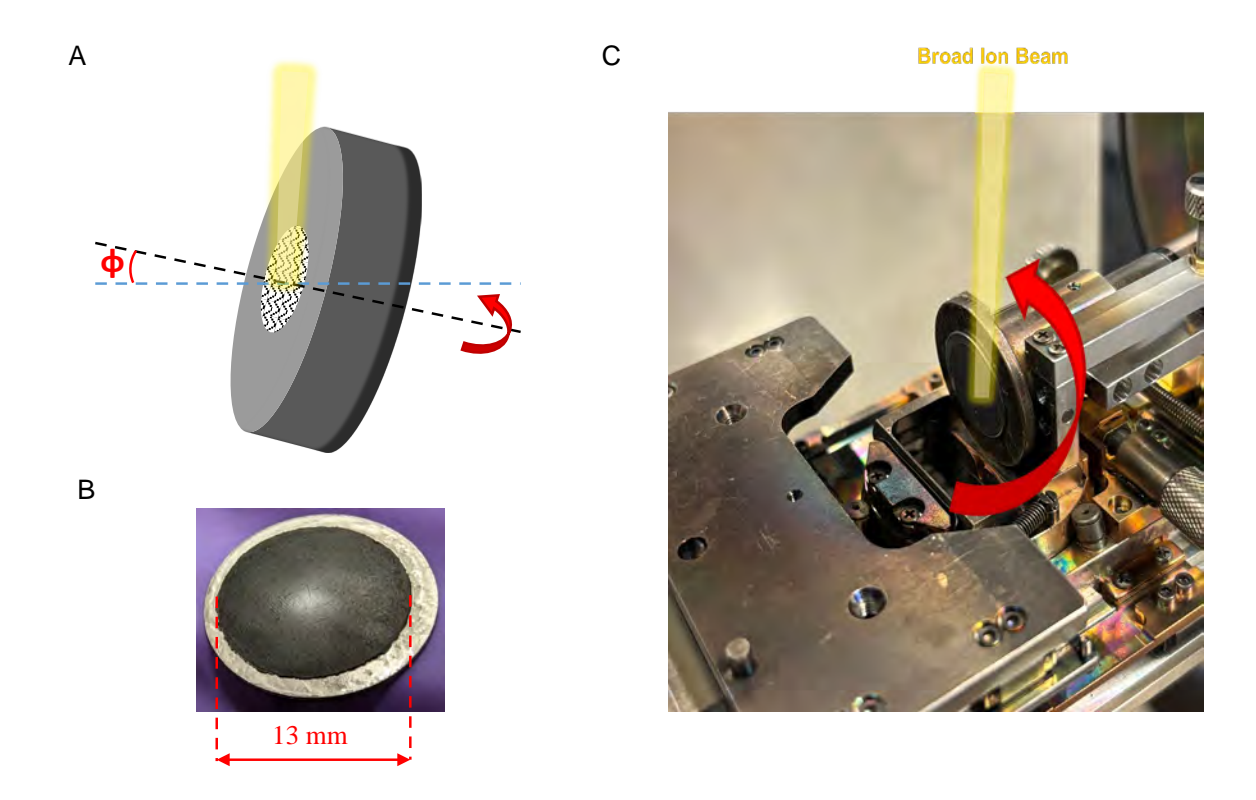


Fig. S1. Surface polishing of NMC cathodes. (A) Schematic of broad ion beam polishing where the Ar-beam hits the rotating sample at the center region. The sample axis (black dashed line) is tilted by an angle Φ with respect to the horizontal axis (blue dotted line) of the ion polishing machine. The sample rotates about its axis. (B) An NMC cathode sample after polishing. (C) A snapshot of surface polishing where the cathode is attached to the sample holder and the surface is kept parallel to the ion beam. The argon flow rate, accelerating voltage, milling time, and Φ are optimized by trial and error experiments.

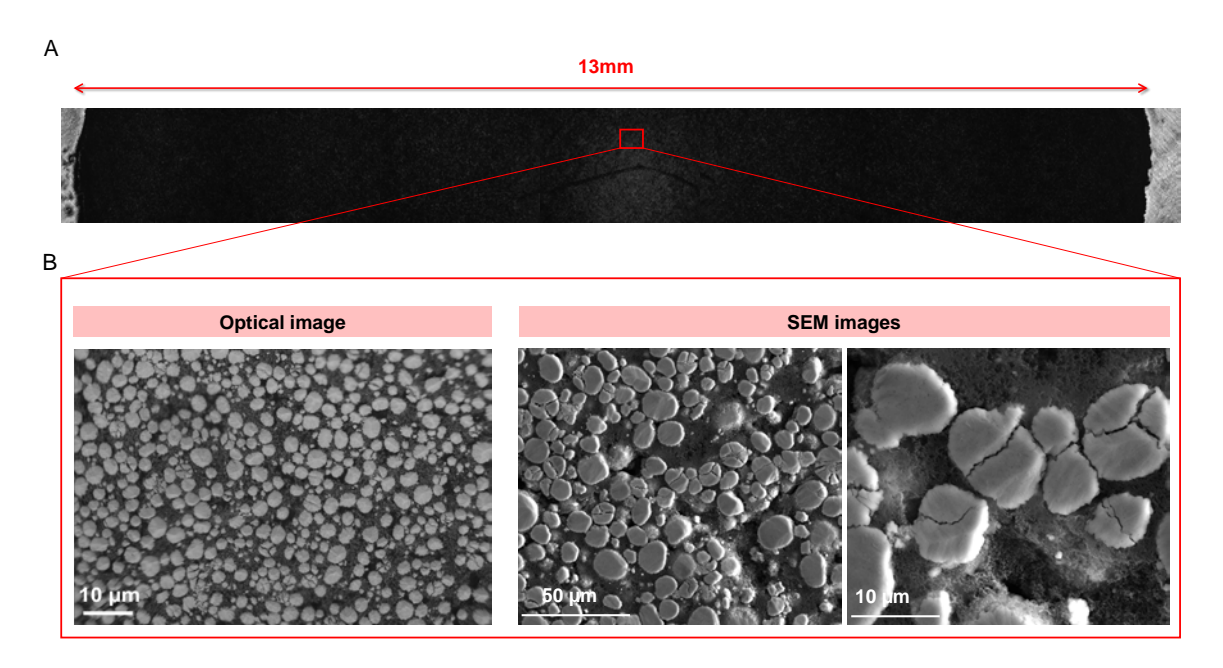


Fig. S2. Optical and scanning electron microscope (SEM) images of a polished NMC sample. (A) A large field of view optical image showing the top surface of a NMC532 sample with the center polished region. (B) An optical image of the polished NMC cathode taken by a 50X optical lens. Right panels show the same polished region using SEM images. NMC particles are light grey embedded in a porous carbon binder matrix. The active particles are mostly spherical and have a diameter of 1-10 micrometers.

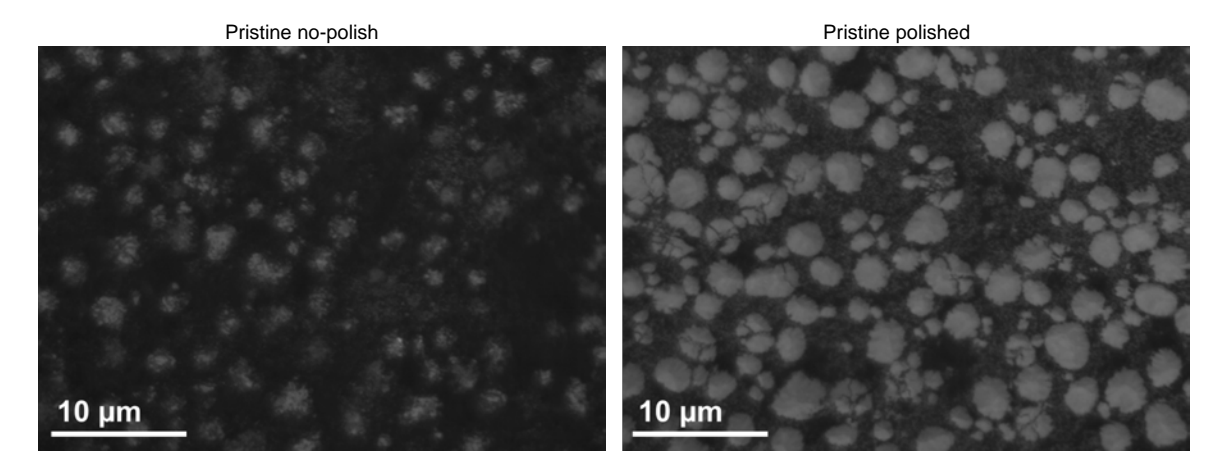


Fig. S3. Optical images at 100X show the comparison of a NMC532 sample before and after polishing.

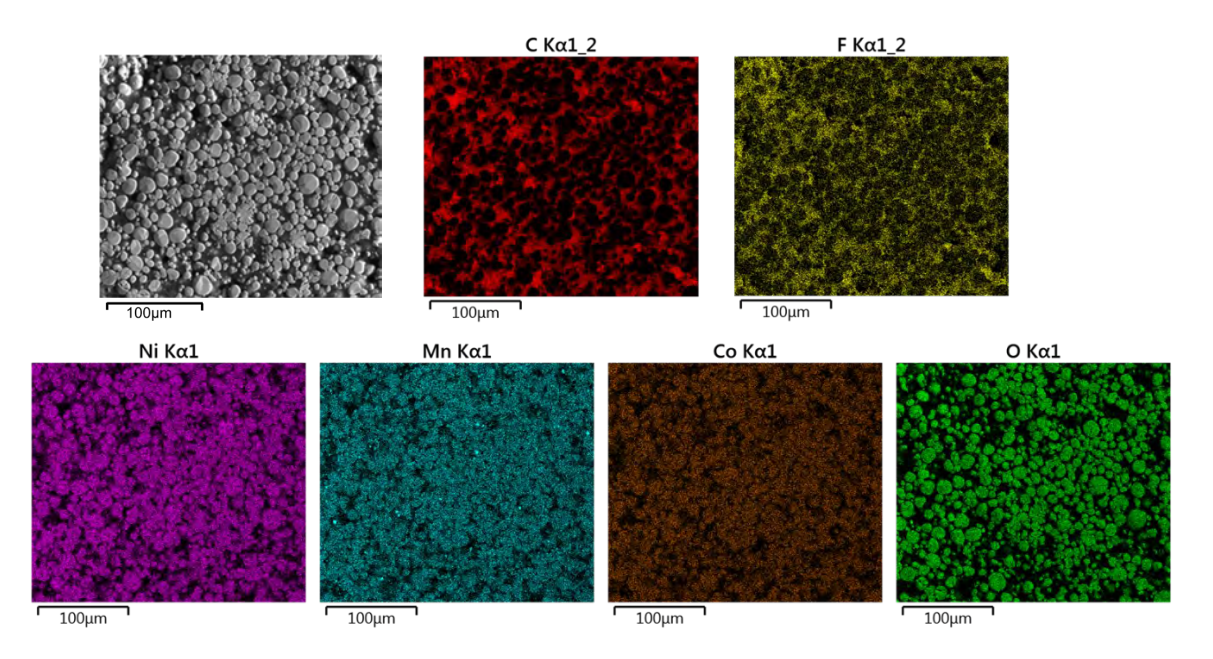


Fig. S4. Energy dispersive X-ray spectroscopy (EDX) elemental mapping (Carbon, Fluorine, Nickel, Manganese, Cobalt, and Oxygen) of a polished NMC532 cathode surface. Carbon and Fluorine maps correspond to the carbon binders while Oxygen and transition metal (TM) maps correspond to NMC.

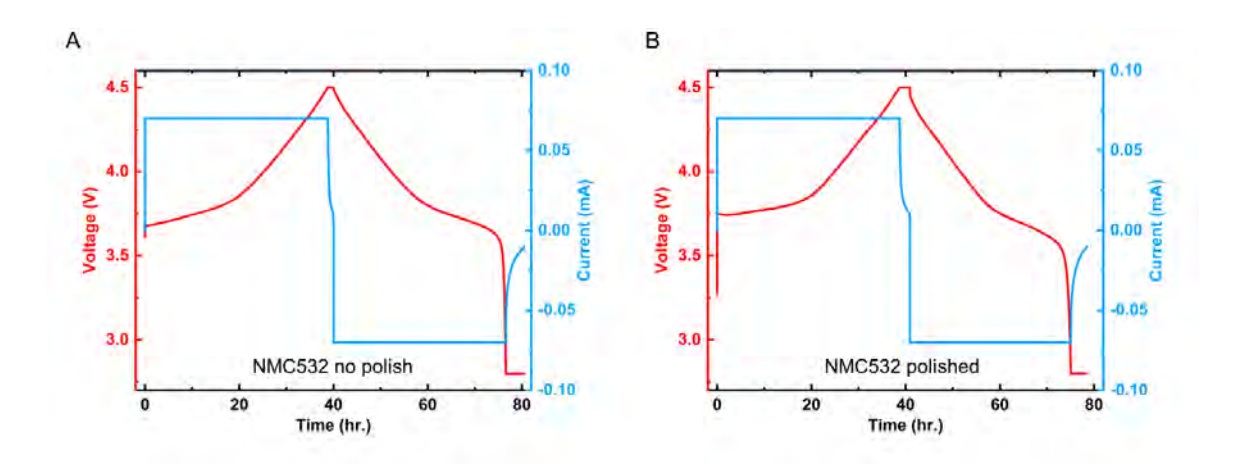


Fig. S5. Voltage-current curves in the first cycle of coin cells using unpolished and polished NMC532 cathode at C/40.

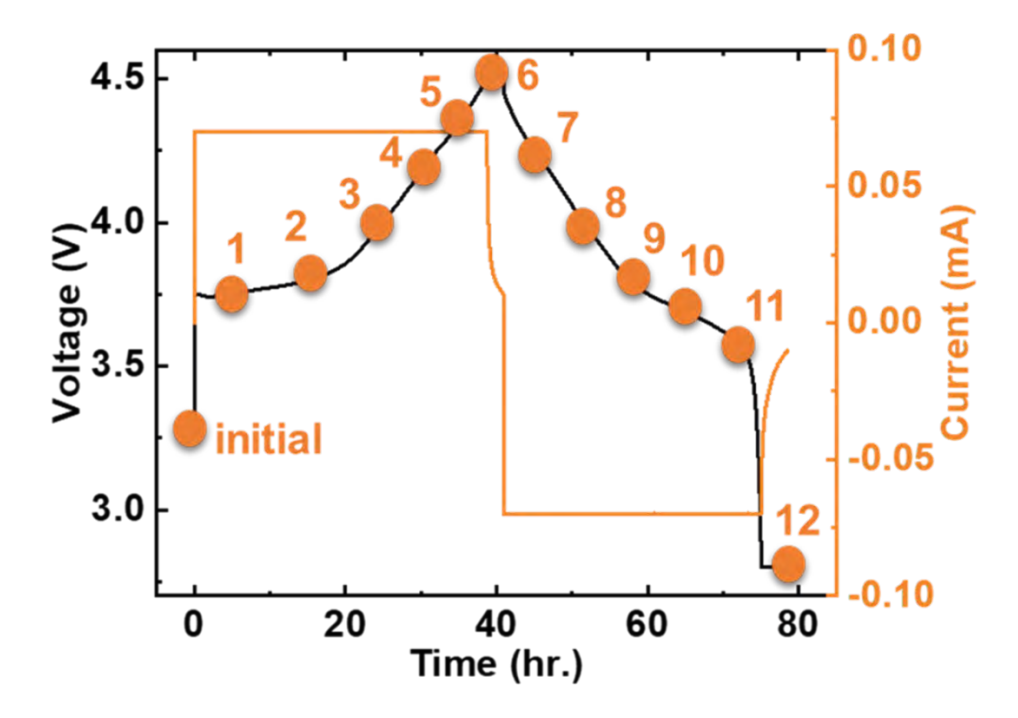


Fig. S6. In ex-situ experiments, polished NMC cathodes are charged and discharged between 2.8 V - 4.5 V at a slow rate (C/40) to attain different voltage stops (orange dots). The coin cells are disassembled at a given voltage, and the state of charge of individual NMC particles is determined using optical microscopy.

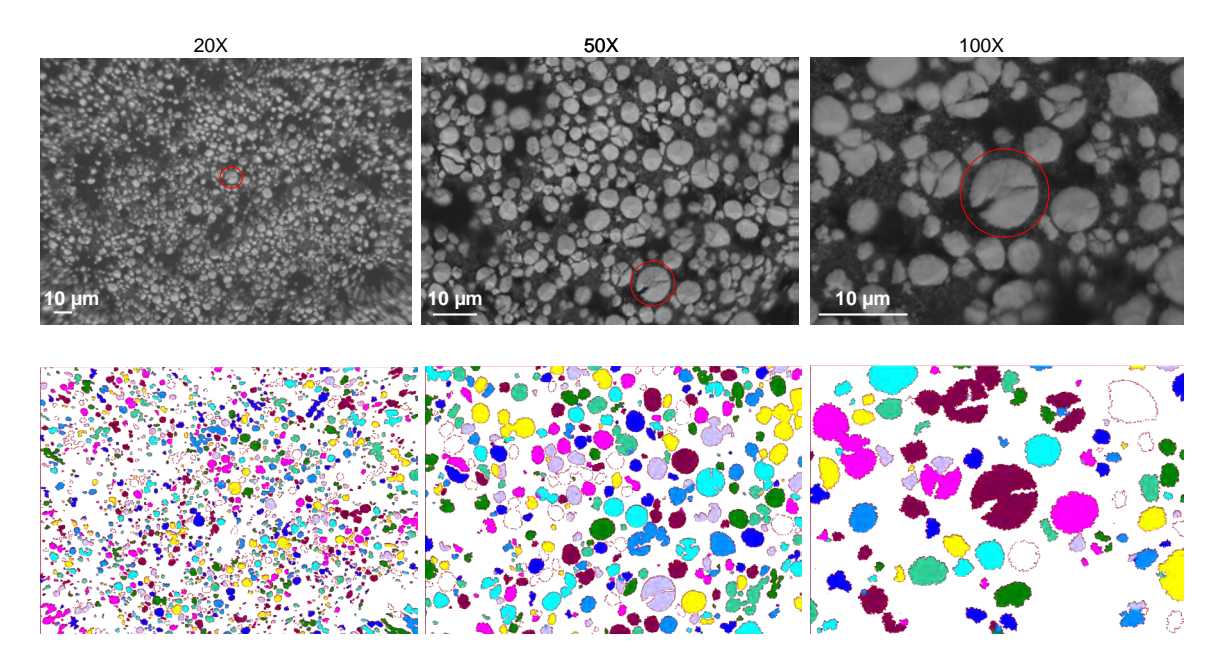


Fig. S7. Image segmentation of NMC particles in the same region using different optical lens (20X, 50X, and 100X). One common particle at the center is marked with a red circle.

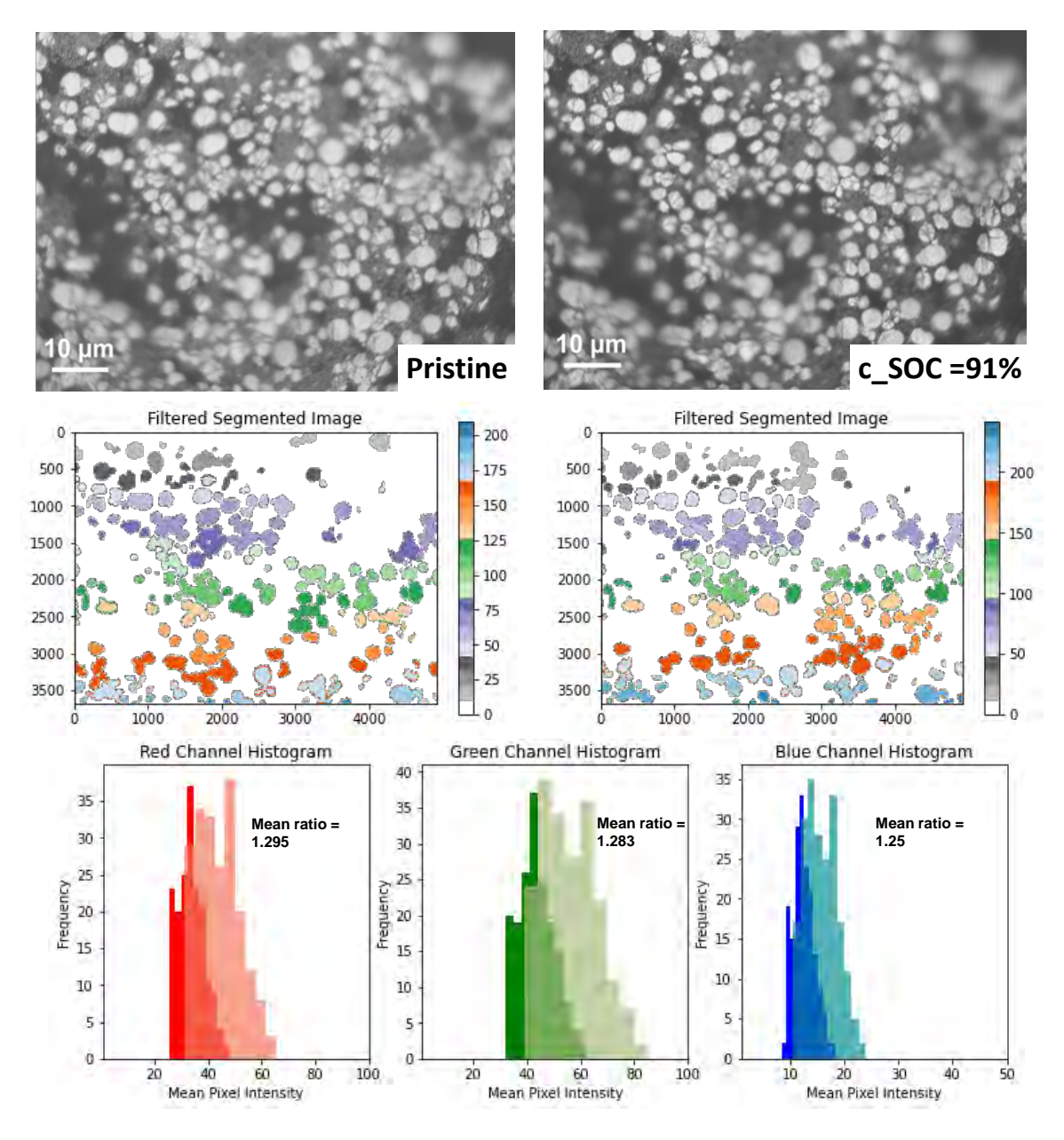


Fig. S8. This figure and Figs. S9-S10 show the robustness of the optical method in extracting the optical properties of NMC particles with different focus settings. The upper panels show 50X optical images of the same region in NMC622 at the pristine state and SOC=91% during charging with focus setting 1. The variation in height of the polished surface often leads to many particles being out of focus. The filtered segmented images are shown in the middle panels, and the mean ratios of red, green, and blue color pixel histograms are shown in the lower panels.

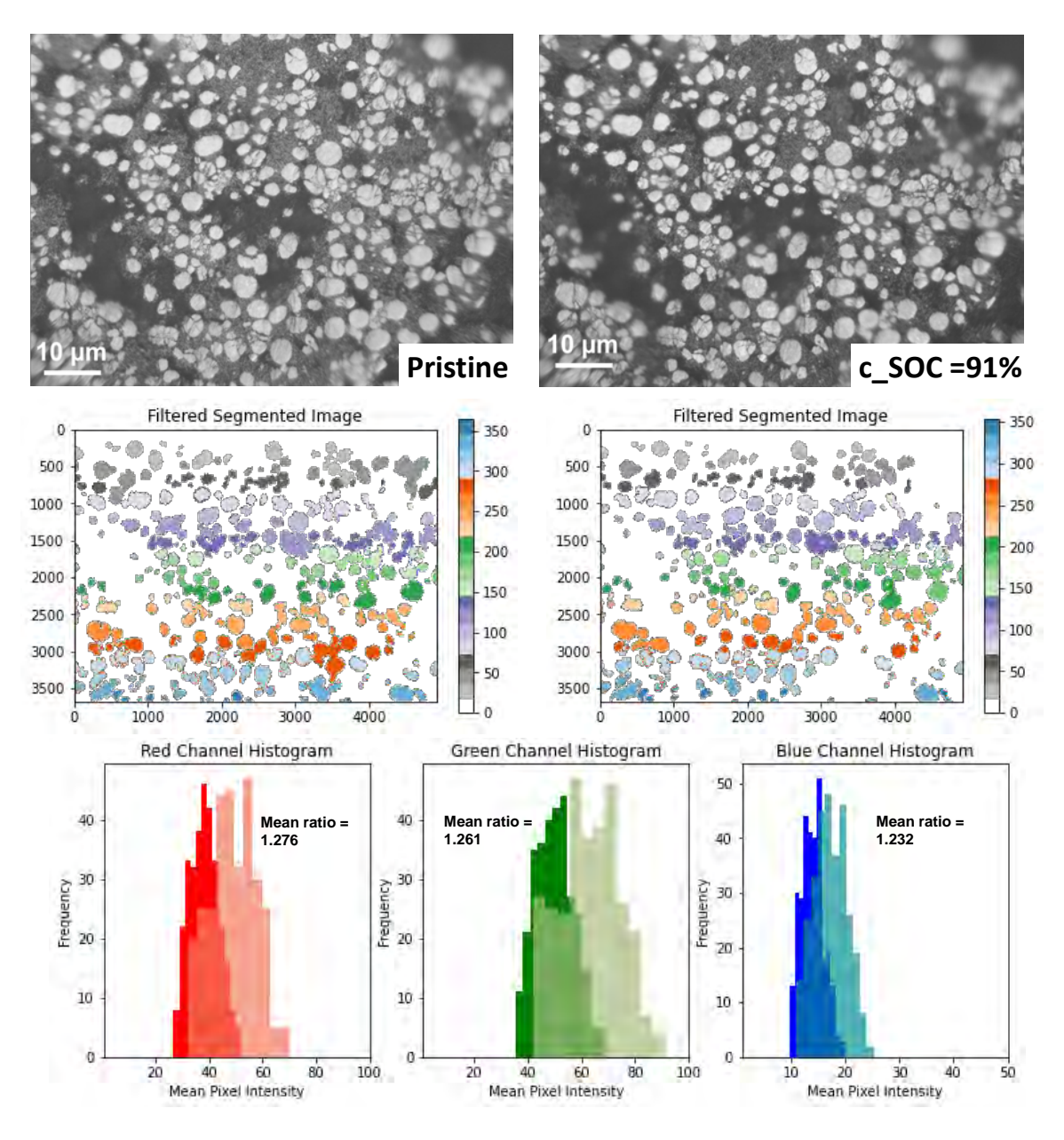


Fig. S9. The upper panels show 50X optical images of the same region in NMC622 at the pristine state and SOC=91% during charging with focus setting 2. Compared to Fig. S8, both images have different particles in focus, which lead to different segmented images as shown in the middle panels. The lower panels show the mean ratios of red, green, and blue color pixel histograms.

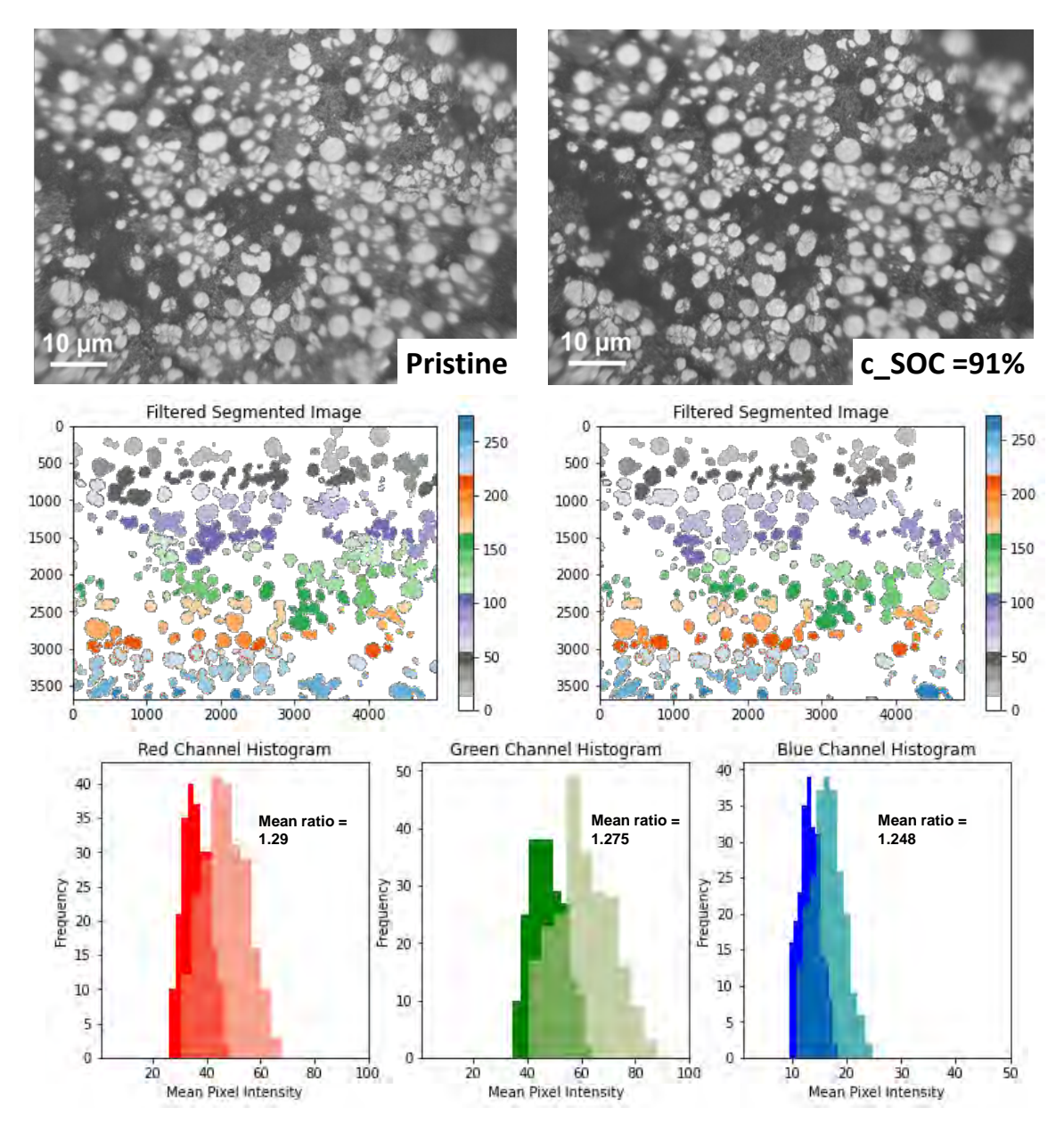


Fig. S10. The upper panels show 50X optical images of the same region at the pristine state and SOC=91% during charging with focus setting 3. The middle panels show segmented images, and the lower panels show the mean ratios of red, green, and blue color pixel histograms.

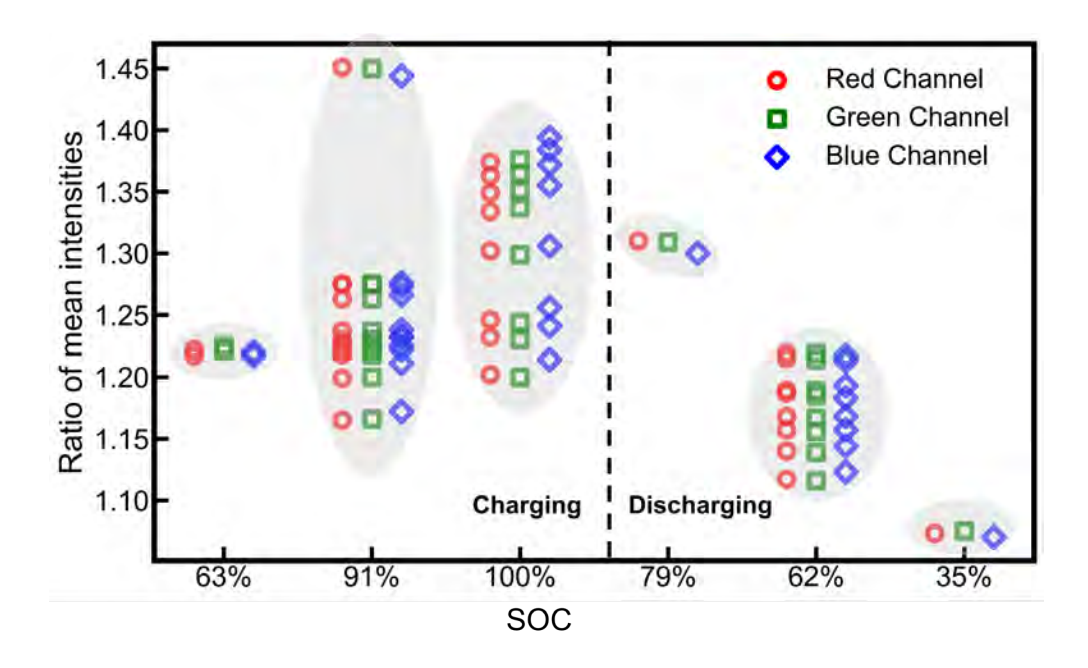


Fig. S11. Optical intensities of NMC particles at different voltage stops with the small FOV at 50X. Coin cells are disassembled at a given voltage (SOC) and normalized optical intensities of NMC622 particles by their initial values at the pristine state are plotted at different SOCs. The red, green, and blue symbols mark their respective RGB values. Each symbol represents one optical image taken at a given SOC at 50X.

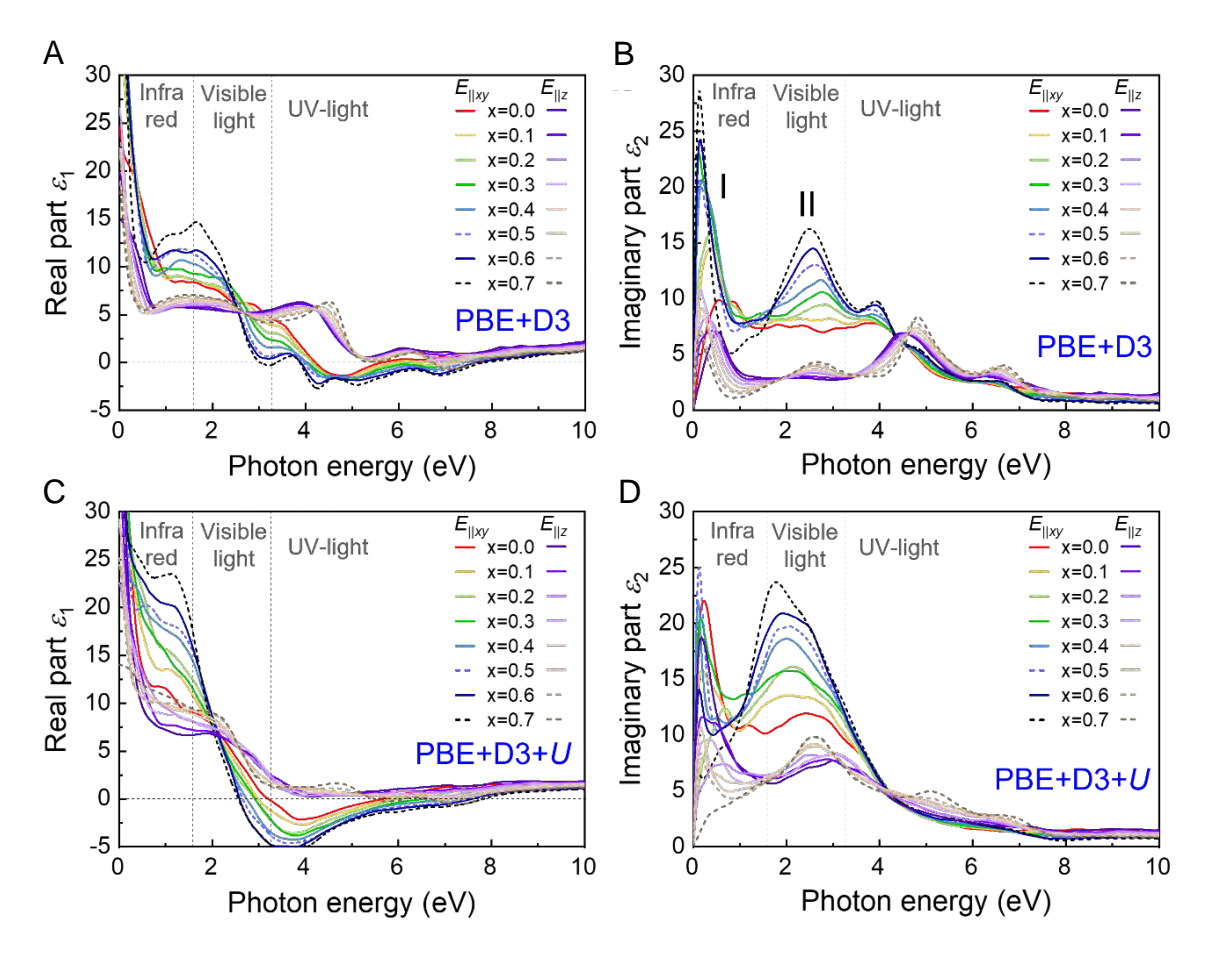


Fig. S12. The real (A, C) and imaginary parts (B, D) of the complex dielectric constant as a function of photon energy for NMC811 at different SOCs, where x = 0 represents the pristine state and x = 0.7 represents the highest delithiation state. Upper panels (A, C) use GGA+D3 functionals, and lower panels show GGA+D3+U results. The permittivity is calculated along both ab- plane and c- axis.

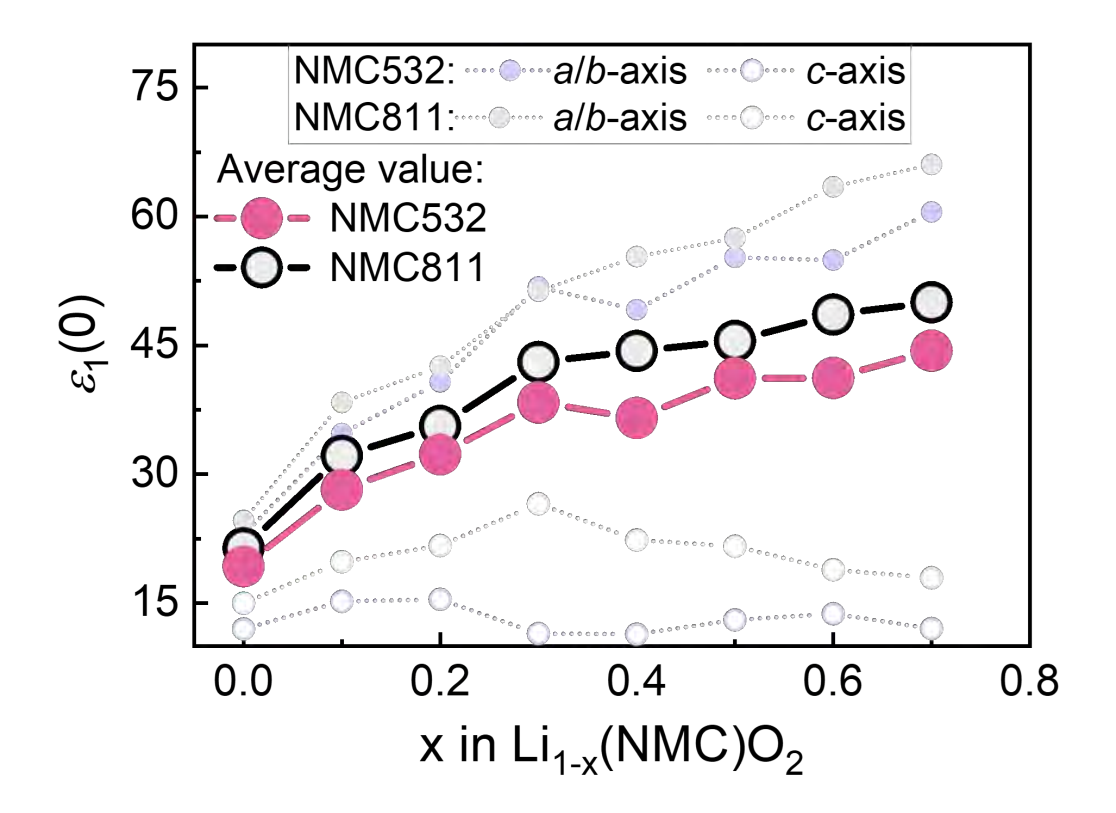


Fig. S13. Static dielectric constant $\varepsilon_1(0)$ as a function of the delithiation state x for NMC811 and NMC532. The plot shows its values along ab- plane and c- axis, and the average.

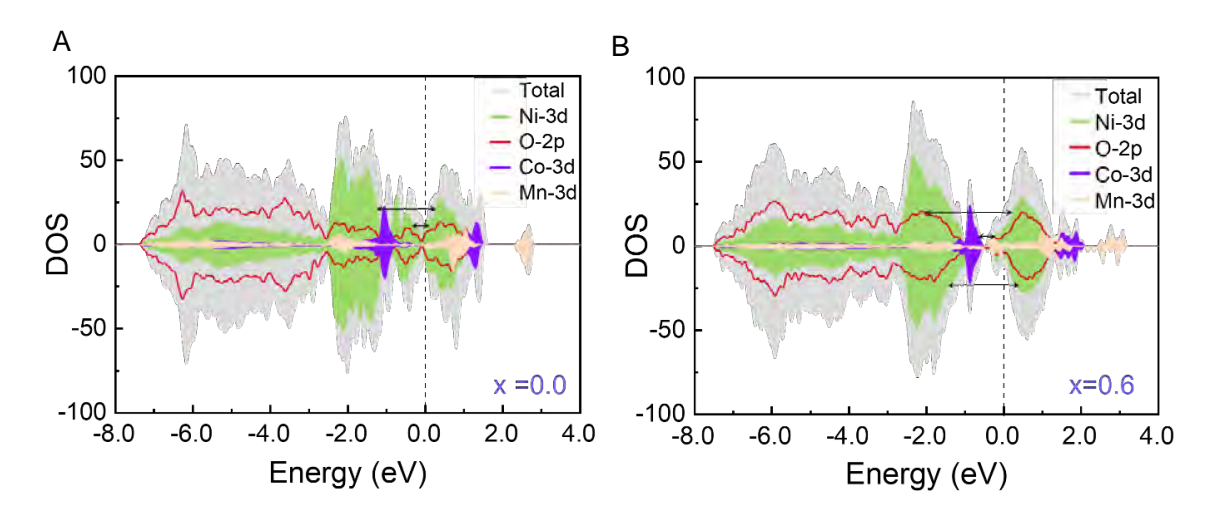


Fig. S14. Density of states of NMC811 at (A) the pristine state x = 0.0 and (B) the delithiated state x = 0.6, where black arrows show possible electronic transitions.

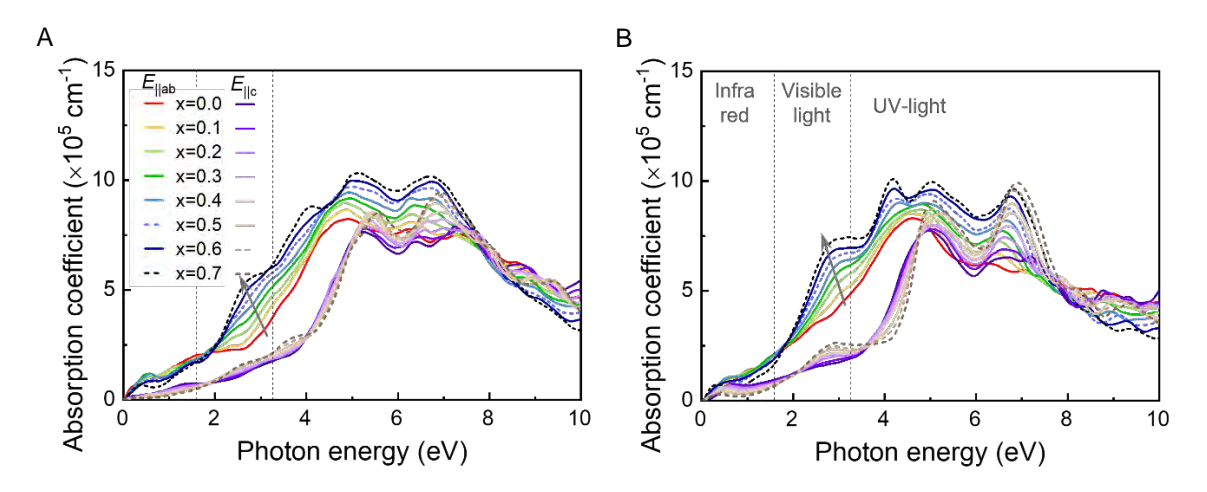


Fig. S15. Optical absorption spectra of (A) NMC532 and (B) NMC811 at different delithiation states.

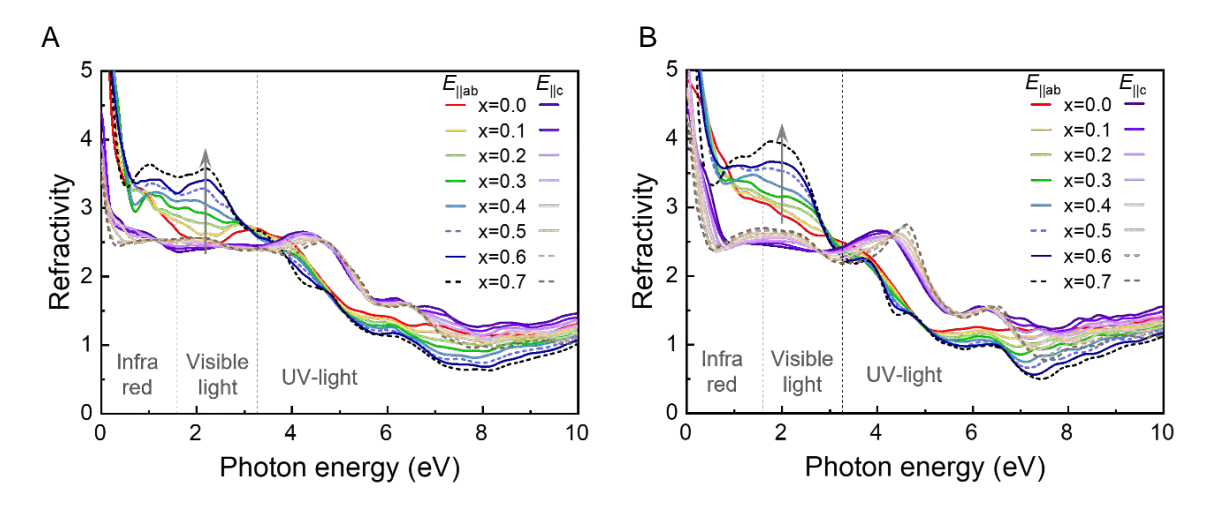


Fig. S16. Optical refractivity of (A) NMC532 and (B) NMC811 at different delithiation states.

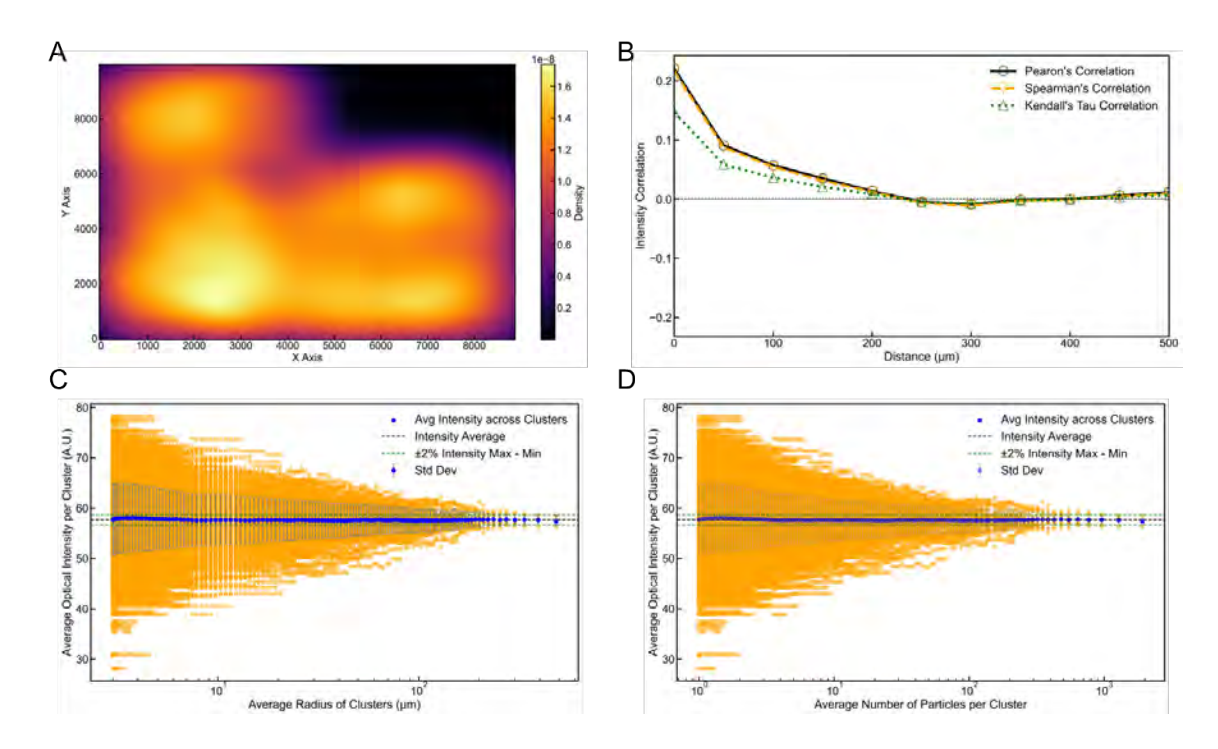


Fig. S17. Optical image analysis of NMC622 at SOC=63% during charging using 20X lens. (A) Kernel Density Estimation (KDE) heatmap of spatial data showing distribution of intensity-weighted datapoints across the coordinate space. Higher density regions (brighter color) correspond to clusters of high-intensity values. (B) Correlation analysis of the optical intensity of NMC particles as a function of spatial distance. Correlation coefficients are calculated within distance bins (width = $10 \mu m$ each) using three metrics: Pearson's, Spearman's, and Kendall's Tau. (C) Convergence of the average optical intensity with the increasing cluster size based on K-Means clustering of spatial coordinates of particle centroid. Blue points represent the mean intensity across clusters at a given spatial scale, and vertical error bars represent the standard deviation. Orange points show individual cluster intensities. Dashed horizontal lines represent global mean intensity (black) and $\pm 2\%$ thresholds (green) relative to the global intensity range. (D) The average optical intensity of NMC particles in a cluster as a function of the average number of particles per cluster.

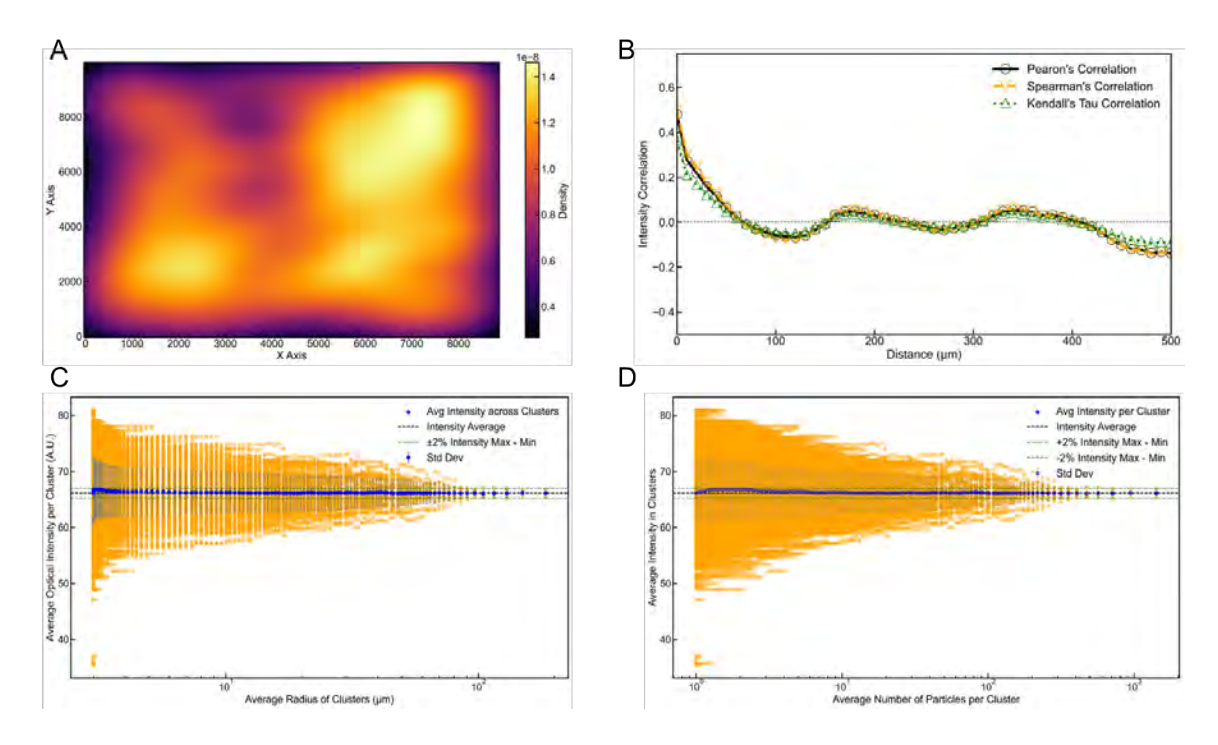


Fig. S18. Optical image analysis of NMC532 at SOC=77% during charging using 50X lens. (A) Kernel Density Estimation (KDE) heatmap of spatial data showing distribution of intensity-weighted datapoints across the coordinate space. Higher density regions (brighter color) correspond to clusters of high-intensity values. (B) Correlation analysis of the optical intensity of NMC particles as a function of spatial distance. Correlation coefficients are calculated within distance bins (width = $10 \mu m$ each) using three metrics: Pearson's, Spearman's, and Kendall's Tau. (C) Convergence of the average optical intensity with the increasing cluster size based on K-Means clustering of spatial coordinates of particle centroid. Blue points represent the mean intensity across clusters at a given spatial scale, and vertical error bars represent the standard deviation. Orange points show individual cluster intensities. Dashed horizontal lines represent global mean intensity (black) and $\pm 2\%$ thresholds (green) relative to the global intensity range. (D) The average optical intensity of NMC particles in a cluster as a function of the average number of particles per cluster.

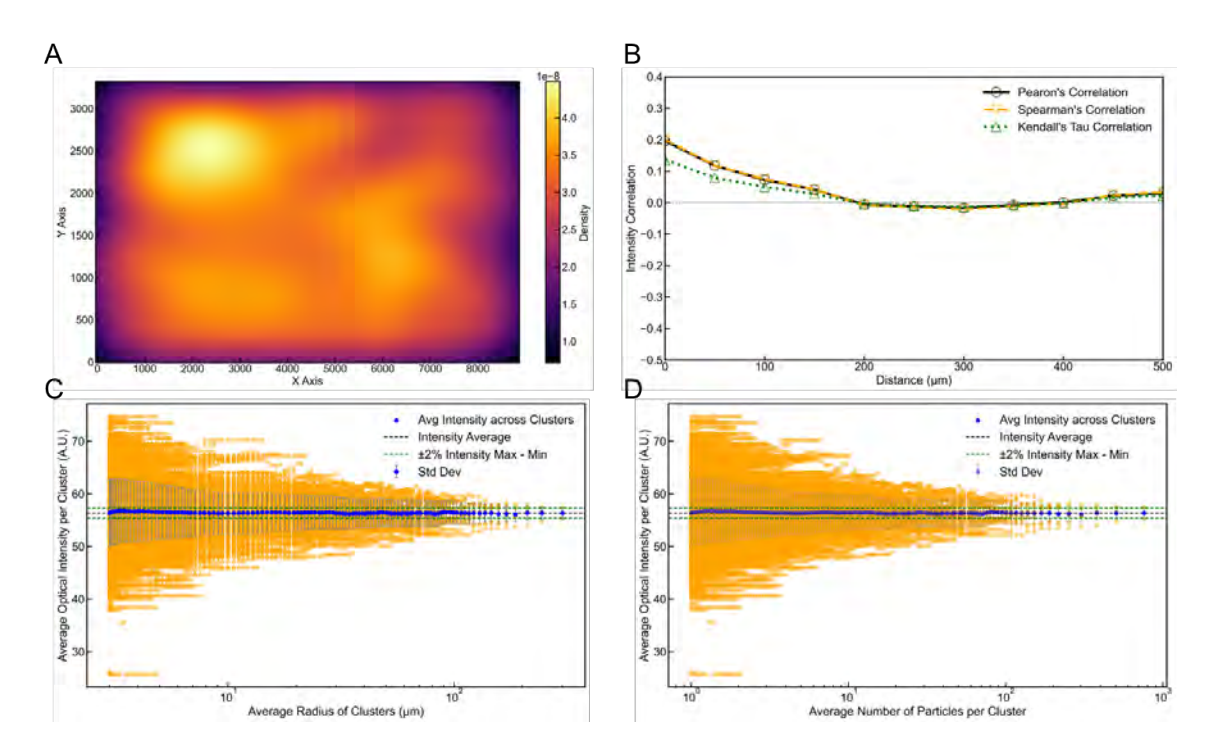


Fig. S19. Optical image analysis of NMC622 at SOC=91% during charging using 20X lens. (A) KDE heatmap of spatial data showing distribution of intensity-weighted datapoints across the coordinate space. Higher density regions (brighter color) correspond to clusters of high-intensity values. (B) Correlation analysis of the optical intensity of NMC particles as a function of spatial distance. Correlation coefficients are calculated within distance bins (width = 10 μ m each) using three metrics: Pearson's, Spearman's, and Kendall's Tau. (C) Convergence of the average optical intensity with the increasing cluster size based on K-Means clustering of spatial coordinates of particle centroid. Blue points represent the mean intensity across clusters at a given spatial scale, and vertical error bars represent the standard deviation. Orange points show individual cluster intensities. Dashed horizontal lines represent global mean intensity (black) and $\pm 2\%$ thresholds (green) relative to the global intensity range. (D) The average optical intensity of NMC particles in a cluster as a function of the average number of particles per cluster.

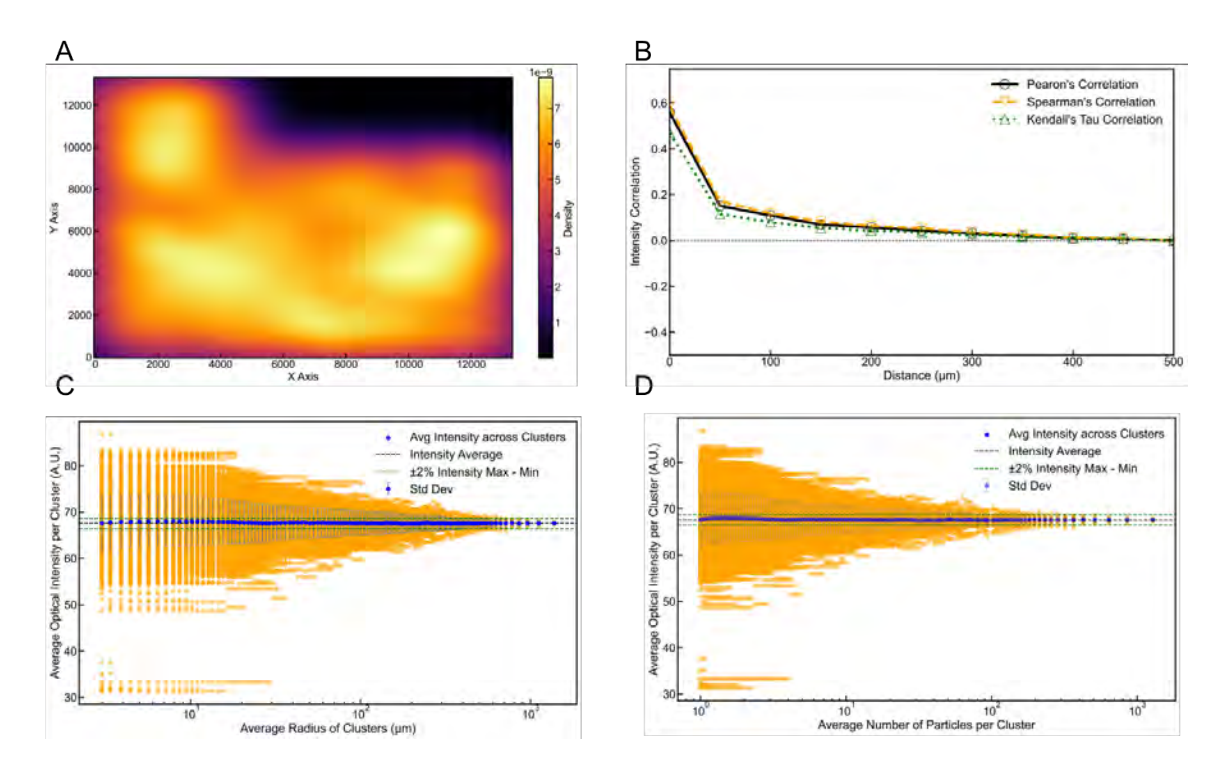


Fig. S20. Optical image analysis of NMC622 at SOC=91% during charging using 40X lens. (A) KDE heatmap of spatial data showing distribution of intensity-weighted datapoints across the coordinate space. Higher density regions (brighter color) correspond to clusters of high-intensity values. (B) Correlation analysis of the optical intensity of NMC particles as a function of spatial distance. Correlation coefficients are calculated within distance bins (width = $10~\mu m$ each) using three metrics: Pearson's, Spearman's, and Kendall's Tau. (C) Convergence of the average optical intensity with the increasing cluster size based on K-Means clustering of spatial coordinates of particle centroid. Blue points represent the mean intensity across clusters at a given spatial scale, and vertical error bars represent the standard deviation. Orange points show individual cluster intensities. Dashed horizontal lines represent global mean intensity (black) and $\pm 2\%$ thresholds (green) relative to the global intensity range. (D) The average optical intensity of NMC particles in a cluster as a function of the average number of particles per cluster.

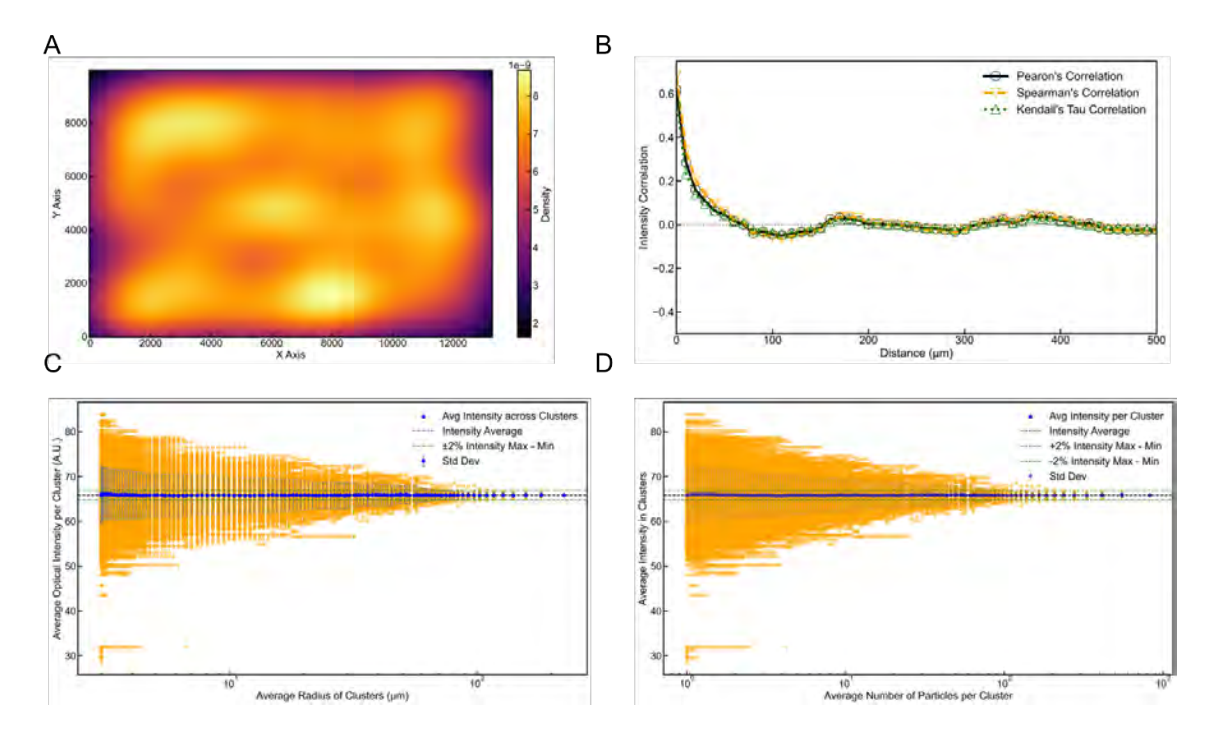


Fig. S21. Optical image analysis of NMC622 at SOC=91% during charging using 50X lens. (A) KDE heatmap of spatial data showing distribution of intensity-weighted datapoints across the coordinate space. Higher density regions (brighter color) correspond to clusters of high-intensity values. (B) Correlation analysis of the optical intensity of NMC particles as a function of spatial distance. Correlation coefficients are calculated within distance bins (width = $10~\mu m$ each) using three metrics: Pearson's, Spearman's, and Kendall's Tau. (C) Convergence of the average optical intensity with the increasing cluster size based on K-Means clustering of spatial coordinates of particle centroid. Blue points represent the mean intensity across clusters at a given spatial scale, and vertical error bars represent the standard deviation. Orange points show individual cluster intensities. Dashed horizontal lines represent global mean intensity (black) and $\pm 2\%$ thresholds (green) relative to the global intensity range. (D) The average optical intensity of NMC particles in a cluster as a function of the average number of particles per cluster.

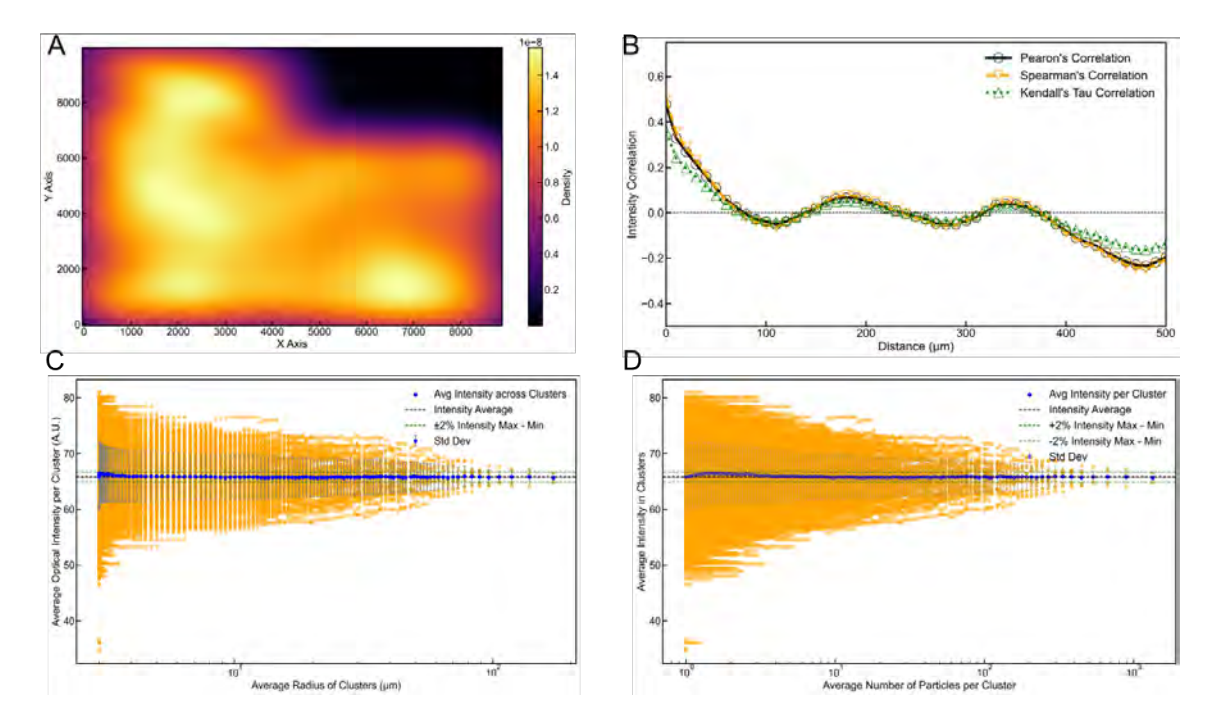


Fig. S22. Optical image analysis of NMC532 at SOC=100% during charging using 50X lens. (A) KDE heatmap of spatial data showing distribution of intensity-weighted datapoints across the coordinate space. Higher density regions (brighter color) correspond to clusters of high-intensity values. (B) Correlation analysis of the optical intensity of NMC particles as a function of spatial distance. Correlation coefficients are calculated within distance bins (width = $10 \mu m$ each) using three metrics: Pearson's, Spearman's, and Kendall's Tau. (C) Convergence of the average optical intensity with the increasing cluster size based on K-Means clustering of spatial coordinates of particle centroid. Blue points represent the mean intensity across clusters at a given spatial scale, and vertical error bars represent the standard deviation. Orange points show individual cluster intensities. Dashed horizontal lines represent global mean intensity (black) and $\pm 2\%$ thresholds (green) relative to the global intensity range. (D) The average optical intensity of NMC particles in a cluster as a function of the average number of particles per cluster. The average optical properties are not converged because of the poor quality of the optical image.

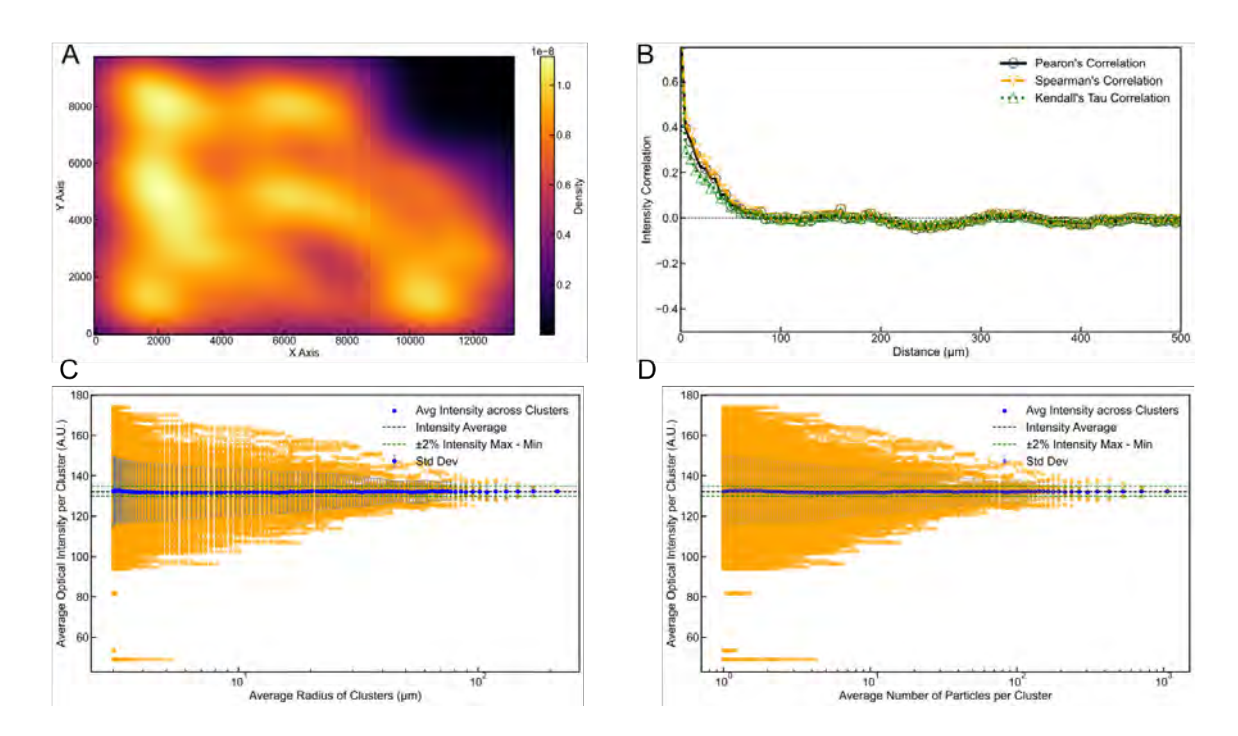


Fig. S23. Optical image analysis of NMC622 at SOC=100% during charging using 50X lens. (A) KDE heatmap of spatial data showing distribution of intensity-weighted datapoints across the coordinate space. Higher density regions (brighter color) correspond to clusters of high-intensity values. (B) Correlation analysis of the optical intensity of NMC particles as a function of spatial distance. Correlation coefficients are calculated within distance bins (width = $10~\mu m$ each) using three metrics: Pearson's, Spearman's, and Kendall's Tau. (C) Convergence of the average optical intensity with the increasing cluster size based on K-Means clustering of spatial coordinates of particle centroid. Blue points represent the mean intensity across clusters at a given spatial scale, and vertical error bars represent the standard deviation. Orange points show individual cluster intensities. Dashed horizontal lines represent global mean intensity (black) and $\pm 2\%$ thresholds (green) relative to the global intensity range. (D) The average optical intensity of NMC particles in a cluster as a function of the average number of particles per cluster.

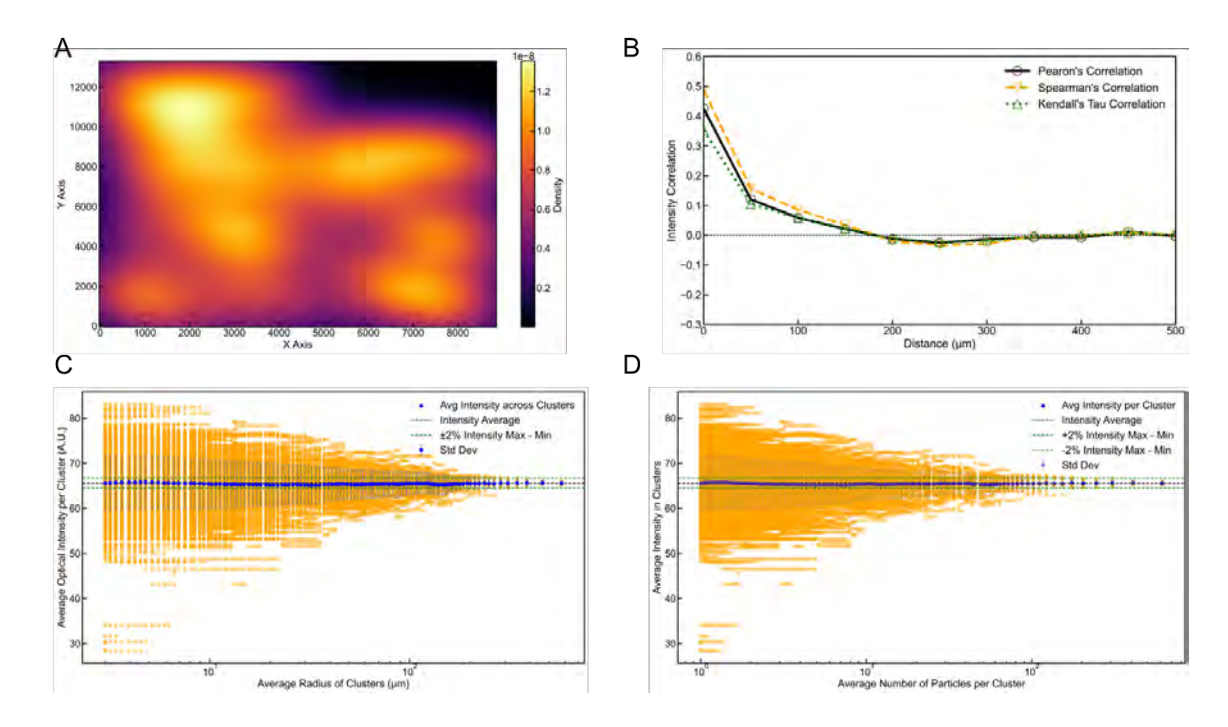


Fig. S24. Optical image analysis of NMC811 at SOC=100% during charging using 20X lens. (A) KDE heatmap of spatial data showing distribution of intensity-weighted datapoints across the coordinate space. Higher density regions (brighter color) correspond to clusters of high-intensity values. (B) Correlation analysis of the optical intensity of NMC particles as a function of spatial distance. Correlation coefficients are calculated within distance bins (width = 10 μ m each) using three metrics: Pearson's, Spearman's, and Kendall's Tau. (C) Convergence of the average optical intensity with the increasing cluster size based on K-Means clustering of spatial coordinates of particle centroid. Blue points represent the mean intensity across clusters at a given spatial scale, and vertical error bars represent the standard deviation. Orange points show individual cluster intensities. Dashed horizontal lines represent global mean intensity (black) and $\pm 2\%$ thresholds (green) relative to the global intensity range. (D) The average optical intensity of NMC particles in a cluster as a function of the average number of particles per cluster.

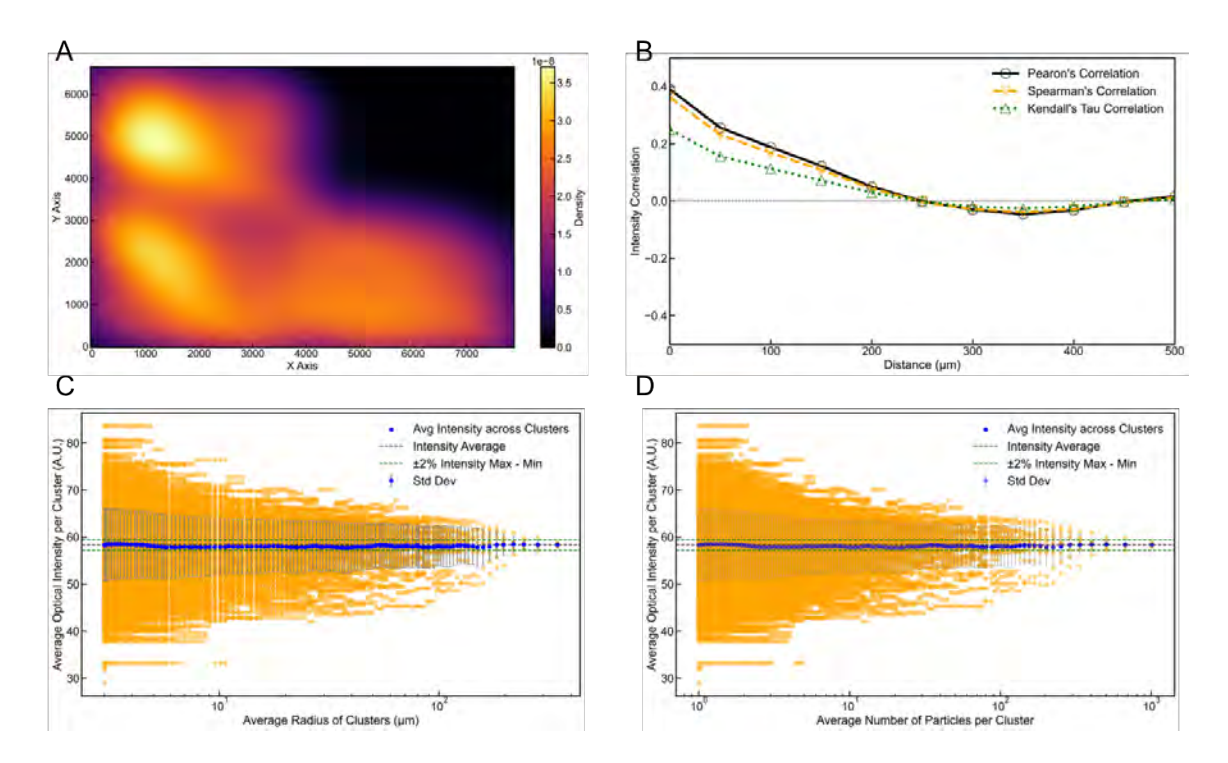


Fig. S25. Optical image analysis of NMC622 at SOC=79% during discharging using 20X lens. (A) KDE heatmap of spatial data showing distribution of intensity-weighted datapoints across the coordinate space. Higher density regions (brighter color) correspond to clusters of high-intensity values. (B) Correlation analysis of the optical intensity of NMC particles as a function of spatial distance. Correlation coefficients are calculated within distance bins (width = $10~\mu m$ each) using three metrics: Pearson's, Spearman's, and Kendall's Tau. (C) Convergence of the average optical intensity with the increasing cluster size based on K-Means clustering of spatial coordinates of particle centroid. Blue points represent the mean intensity across clusters at a given spatial scale, and vertical error bars represent the standard deviation. Orange points show individual cluster intensities. Dashed horizontal lines represent global mean intensity (black) and $\pm 2\%$ thresholds (green) relative to the global intensity range. (D) The average optical intensity of NMC particles in a cluster as a function of the average number of particles per cluster.

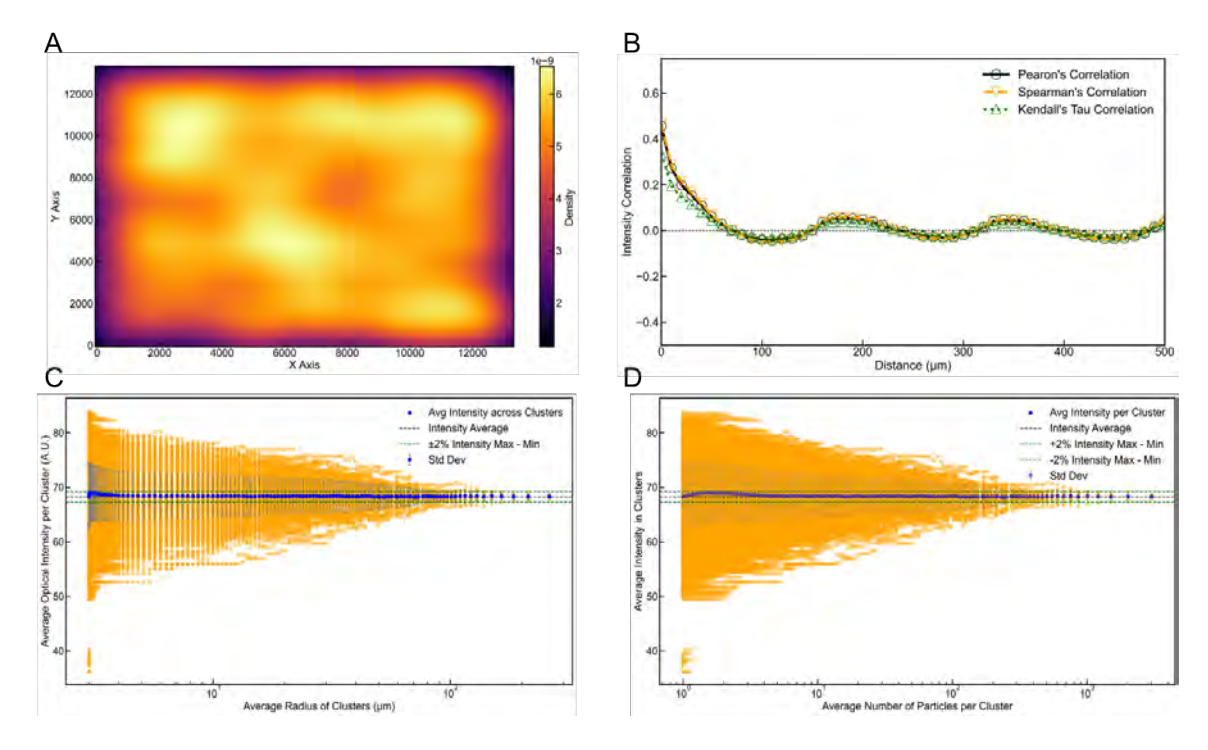


Fig. S26. Optical image analysis of NMC622 at SOC=62% during discharging using 50X lens. (A) KDE heatmap of spatial data showing distribution of intensity-weighted datapoints across the coordinate space. Higher density regions (brighter color) correspond to clusters of high-intensity values. (B) Correlation analysis of the optical intensity of NMC particles as a function of spatial distance. Correlation coefficients are calculated within distance bins (width = $10~\mu m$ each) using three metrics: Pearson's, Spearman's, and Kendall's Tau. (C) Convergence of the average optical intensity with the increasing cluster size based on K-Means clustering of spatial coordinates of particle centroid. Blue points represent the mean intensity across clusters at a given spatial scale, and vertical error bars represent the standard deviation. Orange points show individual cluster intensities. Dashed horizontal lines represent global mean intensity (black) and $\pm 2\%$ thresholds (green) relative to the global intensity range. (D) The average optical intensity of NMC particles in a cluster as a function of the average number of particles per cluster.

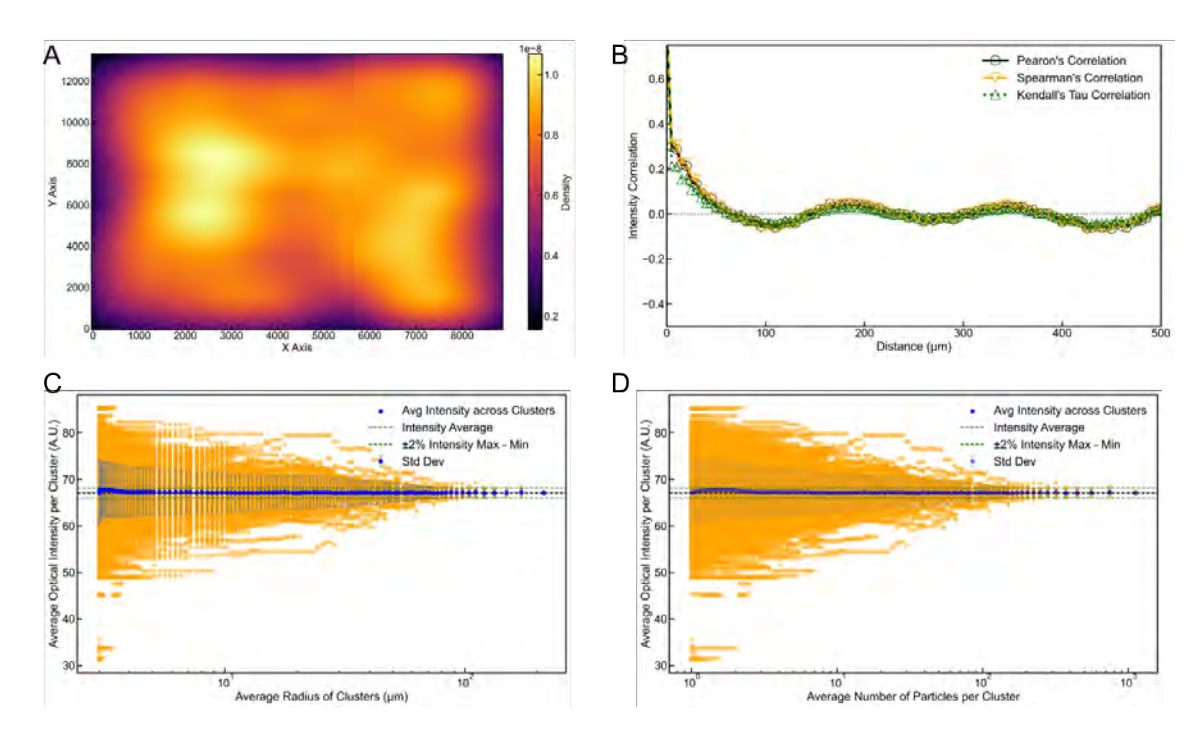


Fig. S27. Optical image analysis of NMC622 at SOC=38% during discharging using 50X lens. (A) KDE heatmap of spatial data showing distribution of intensity-weighted datapoints across the coordinate space. Higher density regions (brighter color) correspond to clusters of high-intensity values. (B) Correlation analysis of the optical intensity of NMC particles as a function of spatial distance. Correlation coefficients are calculated within distance bins (width = $10~\mu m$ each) using three metrics: Pearson's, Spearman's, and Kendall's Tau. (C) Convergence of the average optical intensity with the increasing cluster size based on K-Means clustering of spatial coordinates of particle centroid. Blue points represent the mean intensity across clusters at a given spatial scale, and vertical error bars represent the standard deviation. Orange points show individual cluster intensities. Dashed horizontal lines represent global mean intensity (black) and $\pm 2\%$ thresholds (green) relative to the global intensity range. (D) The average optical intensity of NMC particles in a cluster as a function of the average number of particles per cluster.

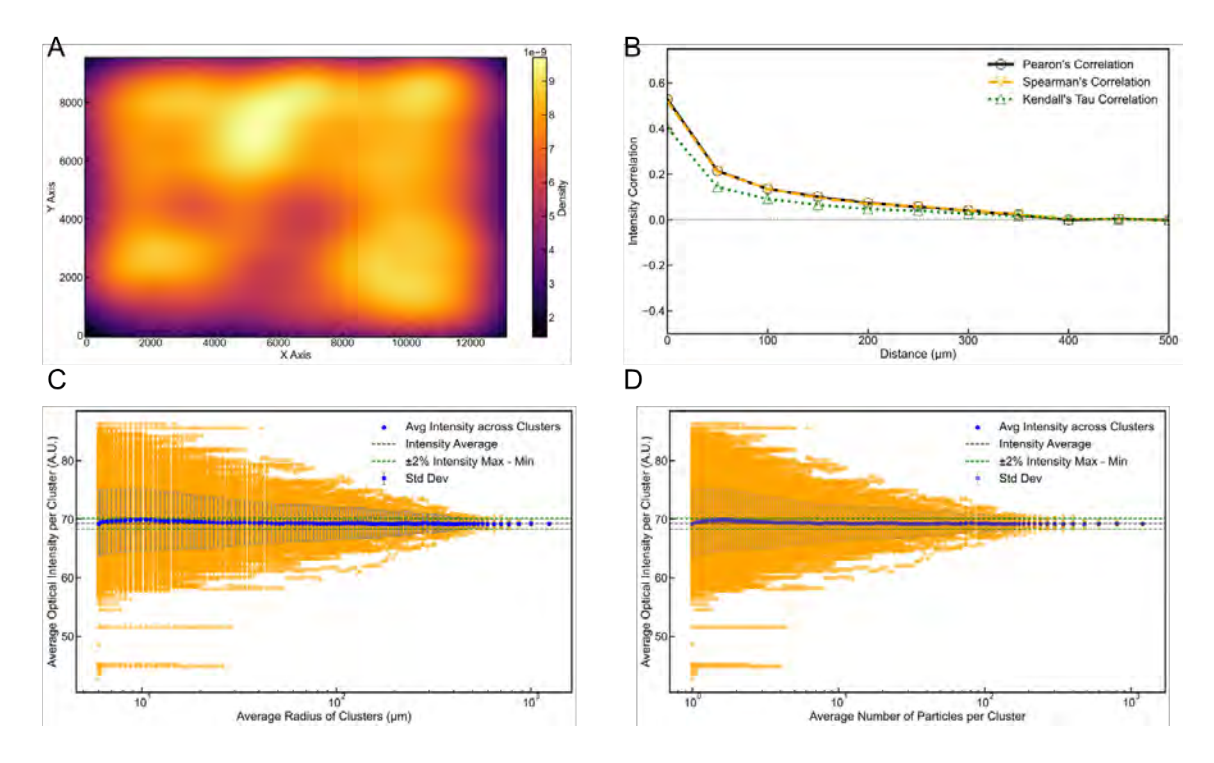


Fig. S28. Optical image analysis of NMC622 at SOC=35% during discharging using 40X lens. (A) KDE heatmap of spatial data showing distribution of intensity-weighted datapoints across the coordinate space. Higher density regions (brighter color) correspond to clusters of high-intensity values. (B) Correlation analysis of the optical intensity of NMC particles as a function of spatial distance. Correlation coefficients are calculated within distance bins (width = $10~\mu m$ each) using three metrics: Pearson's, Spearman's, and Kendall's Tau. (C) Convergence of the average optical intensity with the increasing cluster size based on K-Means clustering of spatial coordinates of particle centroid. Blue points represent the mean intensity across clusters at a given spatial scale, and vertical error bars represent the standard deviation. Orange points show individual cluster intensities. Dashed horizontal lines represent global mean intensity (black) and $\pm 2\%$ thresholds (green) relative to the global intensity range. (D) The average optical intensity of NMC particles in a cluster as a function of the average number of particles per cluster

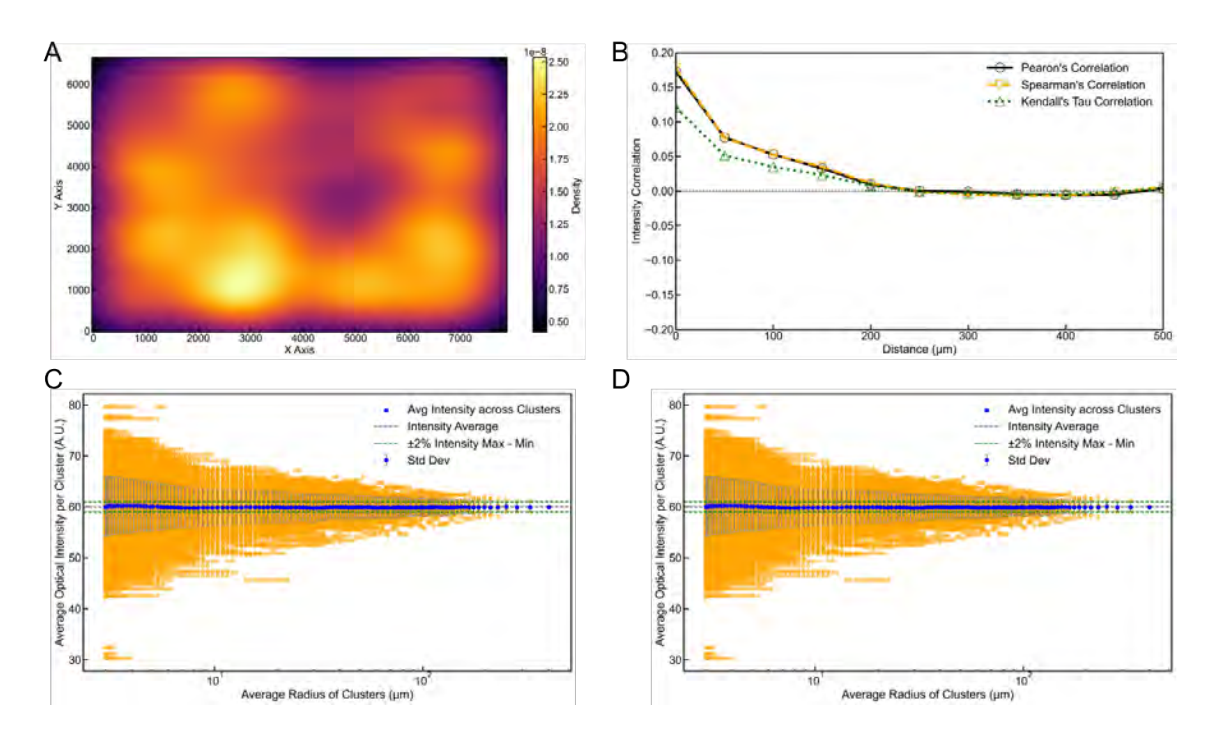


Fig. S29. Optical image analysis of NMC622 at SOC=10% during discharging using 20X lens. (A) KDE heatmap of spatial data showing distribution of intensity-weighted datapoints across the coordinate space. Higher density regions (brighter color) correspond to clusters of high-intensity values. (B) Correlation analysis of the optical intensity of NMC particles as a function of spatial distance. Correlation coefficients are calculated within distance bins (width = 10 μ m each) using three metrics: Pearson's, Spearman's, and Kendall's Tau. (C) Average optical intensity as a function of the increasing cluster size based on K-Means clustering of spatial coordinates of particle centroid. Blue points represent the mean intensity across clusters at a given spatial scale, and vertical error bars represent the standard deviation. Orange points show individual cluster intensities. Dashed horizontal lines represent global mean intensity (black) and $\pm 2\%$ thresholds (green) relative to the global intensity range. (D) The average optical intensity of NMC particles in a cluster as a function of the average number of particles per cluster.

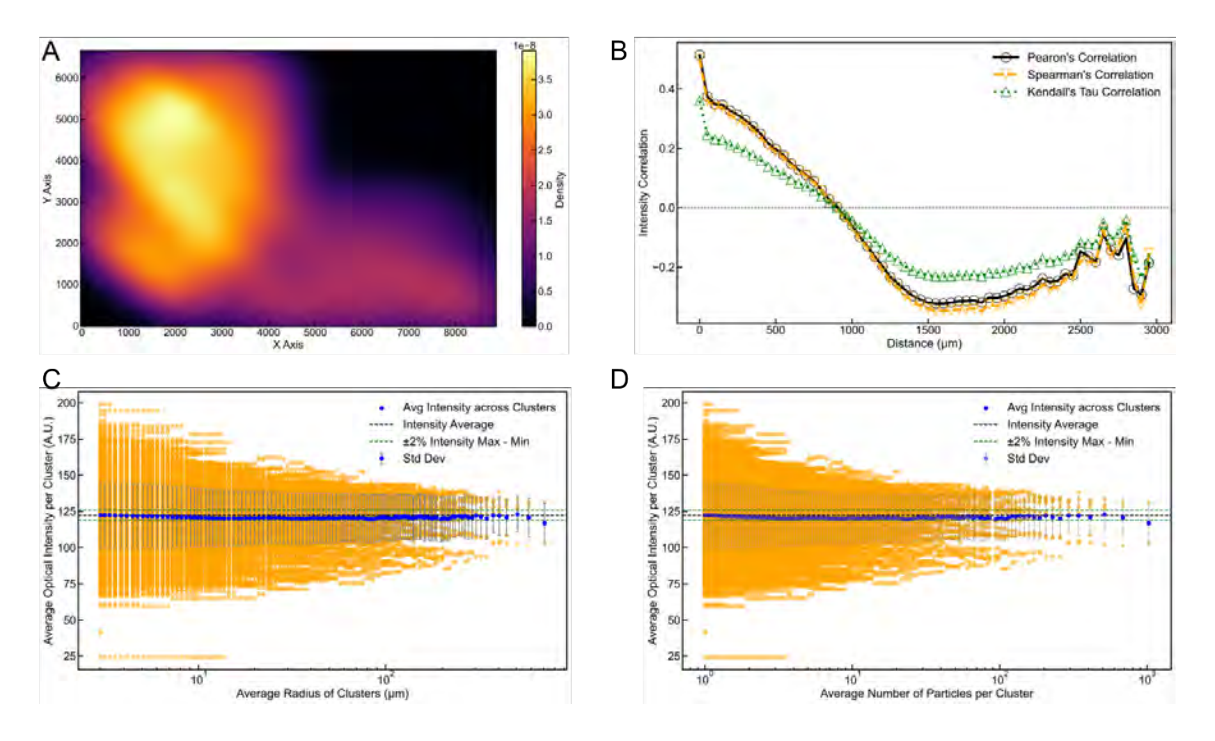


Fig. S30. Optical image analysis of NMC532 at SOC=58% during charging using 40X lens. (A) KDE heatmap of spatial data showing distribution of intensity-weighted datapoints across the coordinate space. Higher density regions (brighter color) correspond to clusters of high-intensity values. (B) Correlation analysis of the optical intensity of NMC particles as a function of spatial distance. Correlation coefficients are calculated within distance bins (width = $10~\mu m$ each) using three metrics: Pearson's, Spearman's, and Kendall's Tau. (C) Average optical intensity as a function of the increasing cluster size based on K-Means clustering of spatial coordinates of particle centroid. Blue points represent the mean intensity across clusters at a given spatial scale, and vertical error bars represent the standard deviation. Orange points show individual cluster intensities. Dashed horizontal lines represent global mean intensity (black) and $\pm 2\%$ thresholds (green) relative to the global intensity range. (D) The average optical intensity of NMC particles in a cluster as a function of the average number of particles per cluster. The average optical properties are not converged because of the poor quality of the optical image.

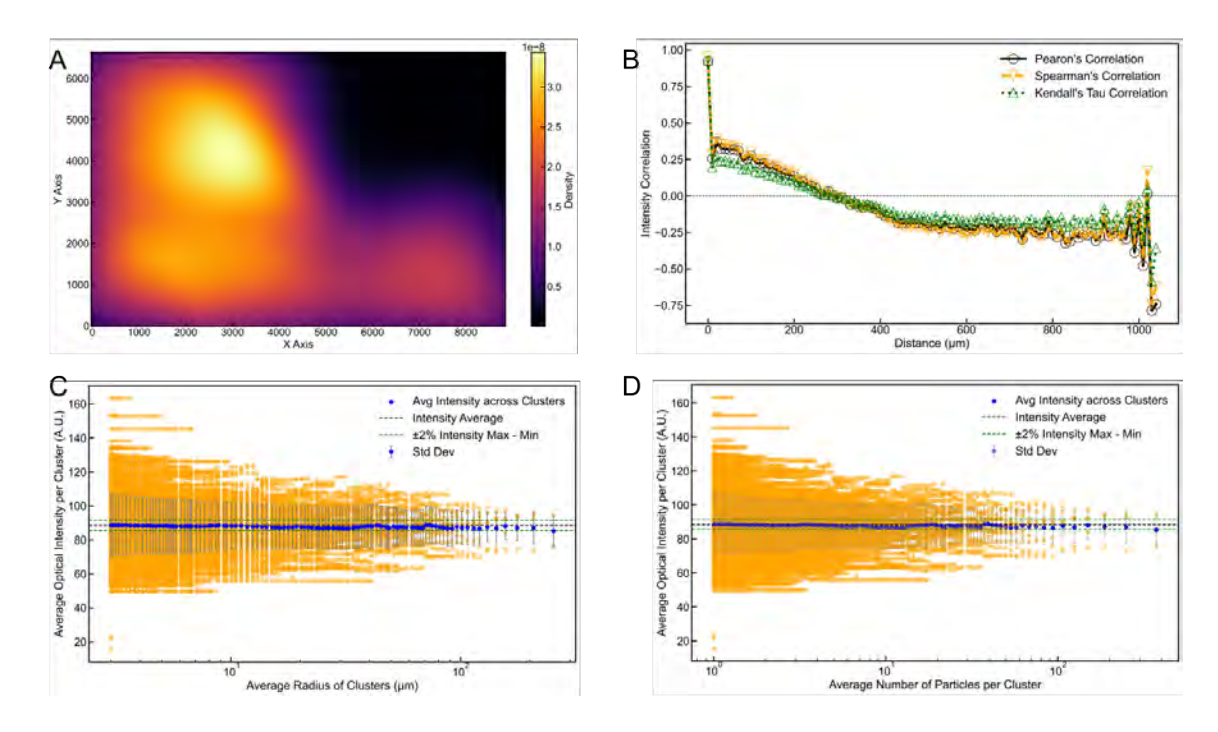


Fig. S31. Optical image analysis of NMC532 at SOC=58% during charging using 100X lens. (A) KDE heatmap of spatial data showing distribution of intensity-weighted datapoints across the coordinate space. Higher density regions (brighter color) correspond to clusters of high-intensity values. (B) Correlation analysis of the optical intensity of NMC particles as a function of spatial distance. Correlation coefficients are calculated within distance bins (width = 10 μ m each) using three metrics: Pearson's, Spearman's, and Kendall's Tau. (C) Average optical intensity as a function of the increasing cluster size based on K-Means clustering of spatial coordinates of particle centroid. Blue points represent the mean intensity across clusters at a given spatial scale, and vertical error bars represent the standard deviation. Orange points show individual cluster intensities. Dashed horizontal lines represent global mean intensity (black) and $\pm 2\%$ thresholds (green) relative to the global intensity range. (D) The average optical intensity of NMC particles in a cluster as a function of the average number of particles per cluster. The average optical properties are not converged because of the poor quality of the optical image.

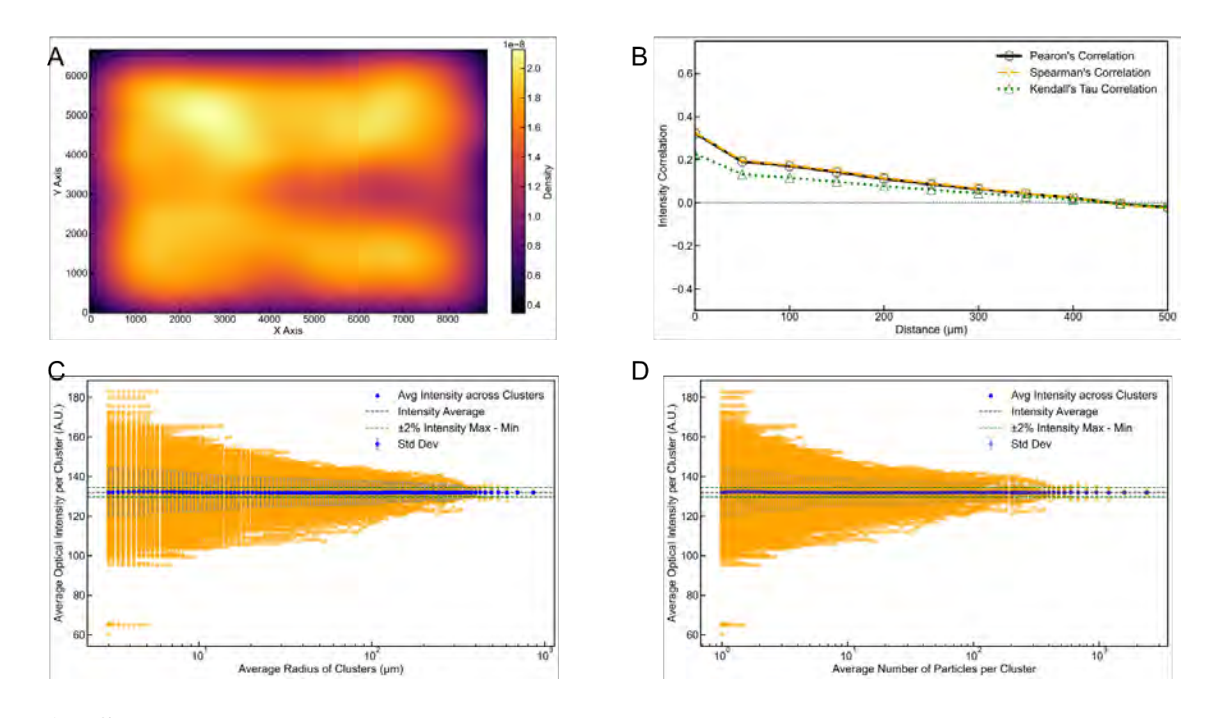


Fig. S32. Optical image analysis of NMC532 at SOC=64% during charging using 40X lens. (A) KDE heatmap of spatial data showing distribution of intensity-weighted datapoints across the coordinate space. Higher density regions (brighter color) correspond to clusters of high-intensity values. (B) Correlation analysis of the optical intensity of NMC particles as a function of spatial distance. Correlation coefficients are calculated within distance bins (width = $10~\mu m$ each) using three metrics: Pearson's, Spearman's, and Kendall's Tau. (C) Average optical intensity as a function of the increasing cluster size based on K-Means clustering of spatial coordinates of particle centroid. Blue points represent the mean intensity across clusters at a given spatial scale, and vertical error bars represent the standard deviation. Orange points show individual cluster intensities. Dashed horizontal lines represent global mean intensity (black) and $\pm 2\%$ thresholds (green) relative to the global intensity range. (D) The average optical intensity of NMC particles in a cluster as a function of the average number of particles per cluster.

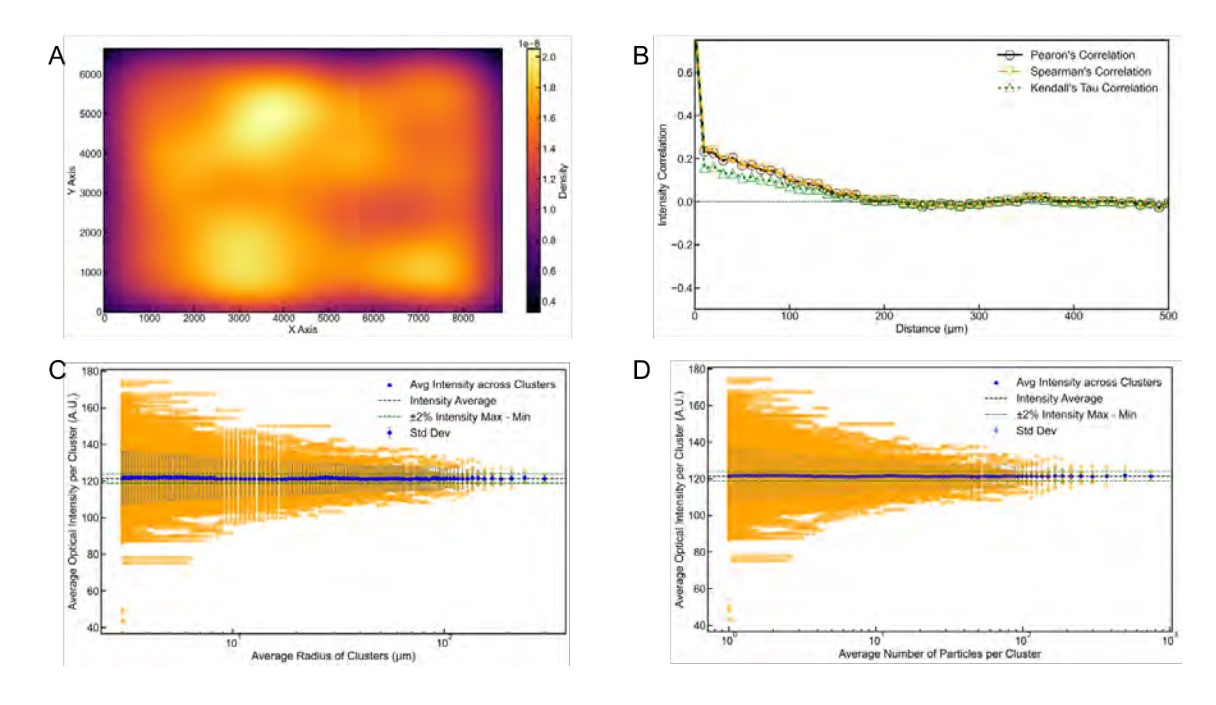


Fig. S33. Optical image analysis of NMC532 at SOC=64% during charging using 100X lens. (A) KDE heatmap of spatial data showing distribution of intensity-weighted datapoints across the coordinate space. Higher density regions (brighter color) correspond to clusters of high-intensity values. (B) Correlation analysis of the optical intensity of NMC particles as a function of spatial distance. Correlation coefficients are calculated within distance bins (width = 10 μ m each) using three metrics: Pearson's, Spearman's, and Kendall's Tau. (C) Average optical intensity as a function of the increasing cluster size based on K-Means clustering of spatial coordinates of particle centroid. Blue points represent the mean intensity across clusters at a given spatial scale, and vertical error bars represent the standard deviation. Orange points show individual cluster intensities. Dashed horizontal lines represent global mean intensity (black) and $\pm 2\%$ thresholds (green) relative to the global intensity range. (D) The average optical intensity of NMC particles in a cluster as a function of the average number of particles per cluster.

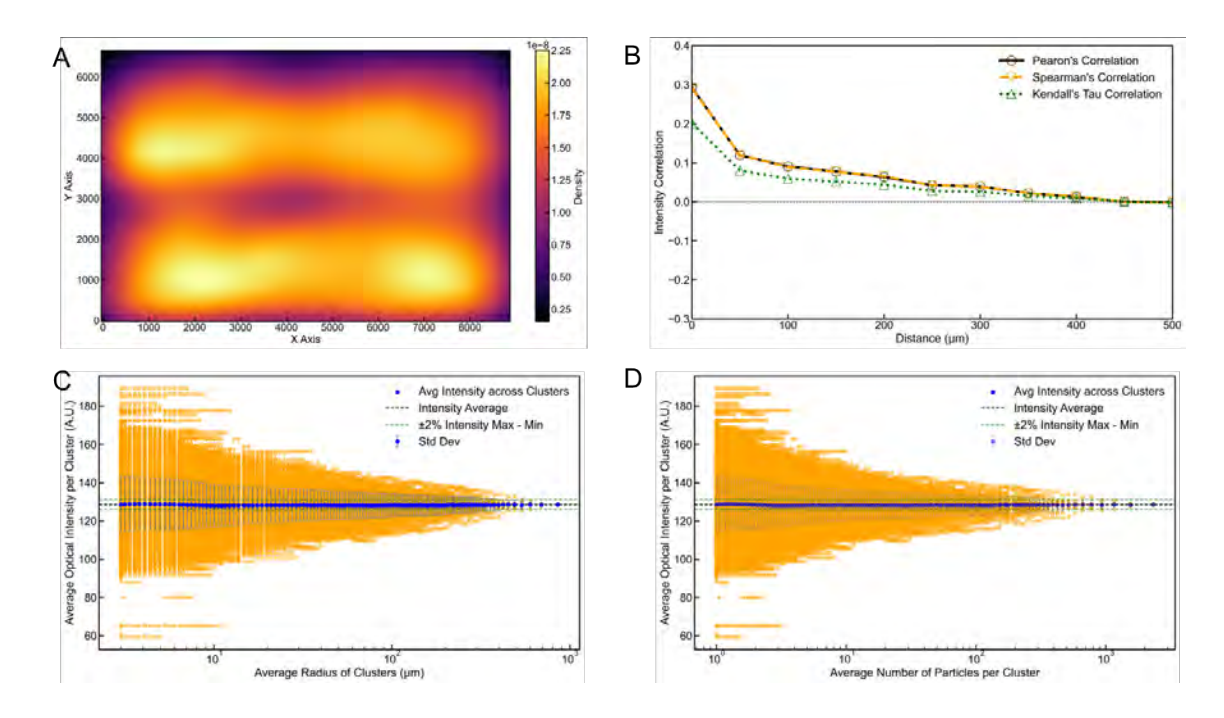


Fig. S34. Optical image analysis of NMC532 at SOC=74% during charging using 40X lens. (A) KDE heatmap of spatial data showing distribution of intensity-weighted datapoints across the coordinate space. Higher density regions (brighter color) correspond to clusters of high-intensity values. (B) Correlation analysis of the optical intensity of NMC particles as a function of spatial distance. Correlation coefficients are calculated within distance bins (width = $10~\mu m$ each) using three metrics: Pearson's, Spearman's, and Kendall's Tau. (C) Average optical intensity as a function of the increasing cluster size based on K-Means clustering of spatial coordinates of particle centroid. Blue points represent the mean intensity across clusters at a given spatial scale, and vertical error bars represent the standard deviation. Orange points show individual cluster intensities. Dashed horizontal lines represent global mean intensity (black) and $\pm 2\%$ thresholds (green) relative to the global intensity range. (D) The average optical intensity of NMC particles in a cluster as a function of the average number of particles per cluster.

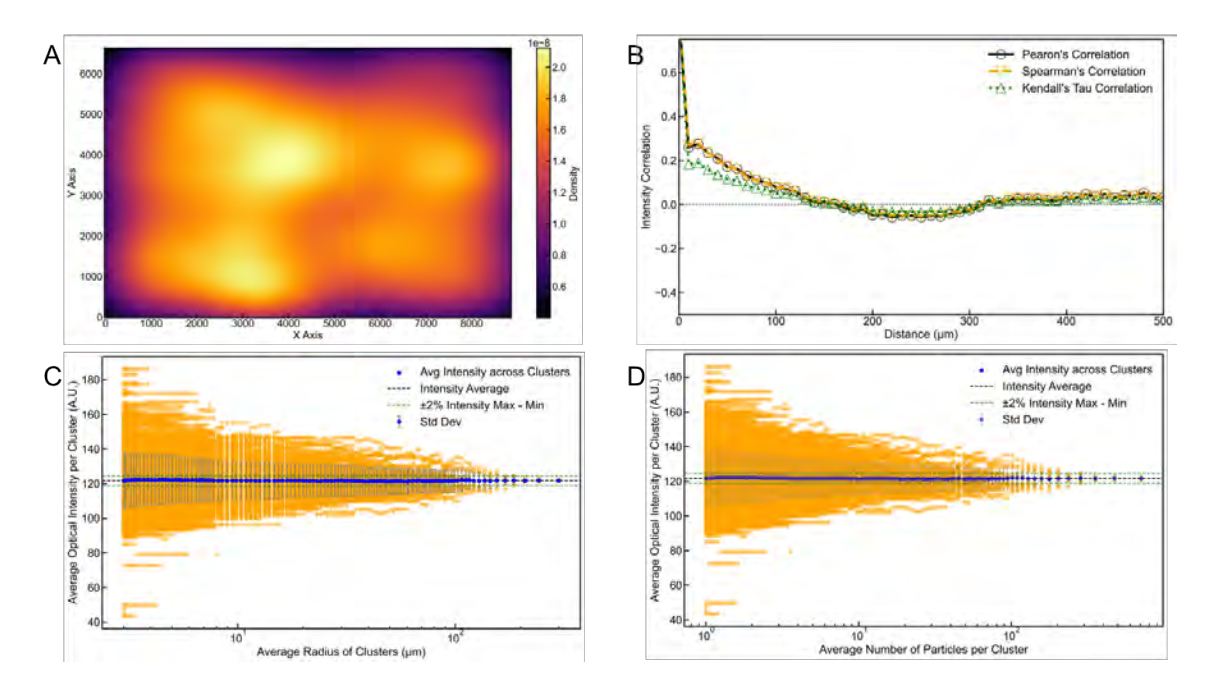


Fig. S35. Optical image analysis of NMC532 at SOC=74% during charging using 100X lens. (A) KDE heatmap of spatial data showing distribution of intensity-weighted datapoints across the coordinate space. Higher density regions (brighter color) correspond to clusters of high-intensity values. (B) Correlation analysis of the optical intensity of NMC particles as a function of spatial distance. Correlation coefficients are calculated within distance bins (width = $10~\mu m$ each) using three metrics: Pearson's, Spearman's, and Kendall's Tau. (C) Average optical intensity as a function of the increasing cluster size based on K-Means clustering of spatial coordinates of particle centroid. Blue points represent the mean intensity across clusters at a given spatial scale, and vertical error bars represent the standard deviation. Orange points show individual cluster intensities. Dashed horizontal lines represent global mean intensity (black) and $\pm 2\%$ thresholds (green) relative to the global intensity range. (D) The average optical intensity of NMC particles in a cluster as a function of the average number of particles per cluster.

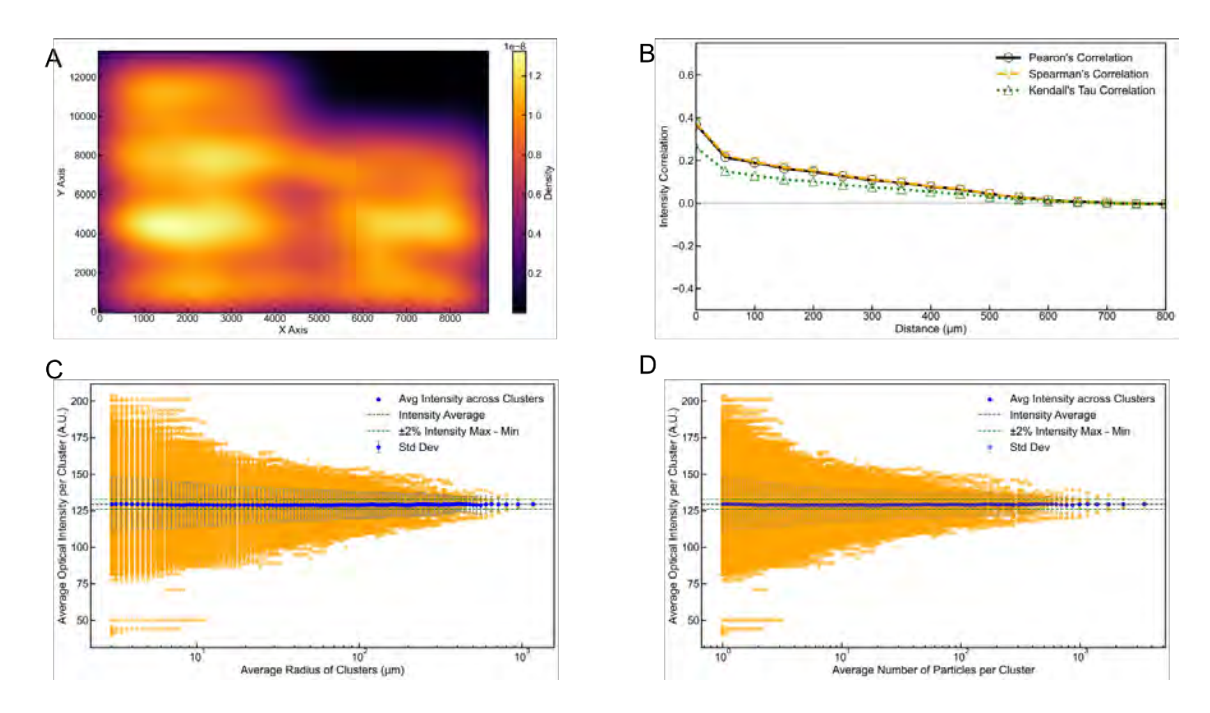


Fig. S36. Optical image analysis of NMC532 at SOC=90% during charging using 40X lens. (A) KDE heatmap of spatial data showing distribution of intensity-weighted datapoints across the coordinate space. Higher density regions (brighter color) correspond to clusters of high-intensity values. (B) Correlation analysis of the optical intensity of NMC particles as a function of spatial distance. Correlation coefficients are calculated within distance bins (width = $10 \mu m$ each) using three metrics: Pearson's, Spearman's, and Kendall's Tau. (C) Average optical intensity as a function of the increasing cluster size based on K-Means clustering of spatial coordinates of particle centroid. Blue points represent the mean intensity across clusters at a given spatial scale, and vertical error bars represent the standard deviation. Orange points show individual cluster intensities. Dashed horizontal lines represent global mean intensity (black) and $\pm 2\%$ thresholds (green) relative to the global intensity range. (D) The average optical intensity of NMC particles in a cluster as a function of the average number of particles per cluster.

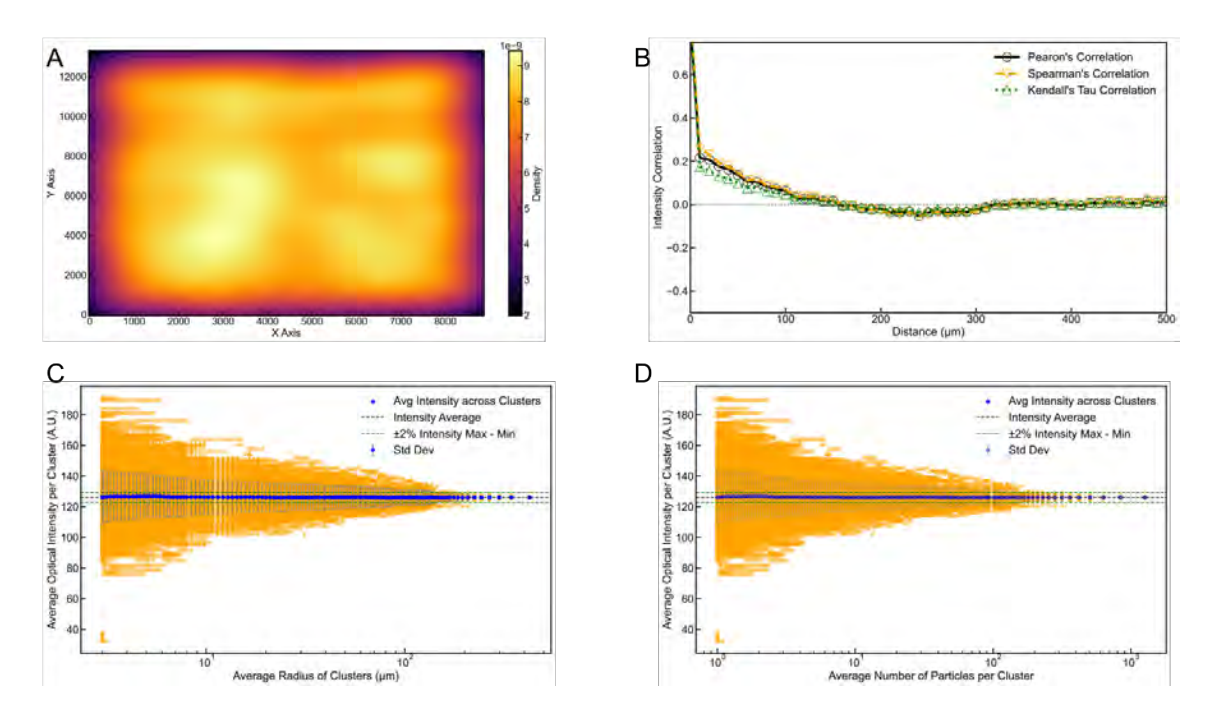


Fig. S37. Optical image analysis of NMC532 at SOC=90% during charging using 100X lens. (A) KDE heatmap of spatial data showing distribution of intensity-weighted datapoints across the coordinate space. Higher density regions (brighter color) correspond to clusters of high-intensity values. (B) Correlation analysis of the optical intensity of NMC particles as a function of spatial distance. Correlation coefficients are calculated within distance bins (width = $10 \mu m$ each) using three metrics: Pearson's, Spearman's, and Kendall's Tau. (C) Average optical intensity as a function of the increasing cluster size based on K-Means clustering of spatial coordinates of particle centroid. Blue points represent the mean intensity across clusters at a given spatial scale, and vertical error bars represent the standard deviation. Orange points show individual cluster intensities. Dashed horizontal lines represent global mean intensity (black) and $\pm 2\%$ thresholds (green) relative to the global intensity range. (D) The average optical intensity of NMC particles in a cluster as a function of the average number of particles per cluster.

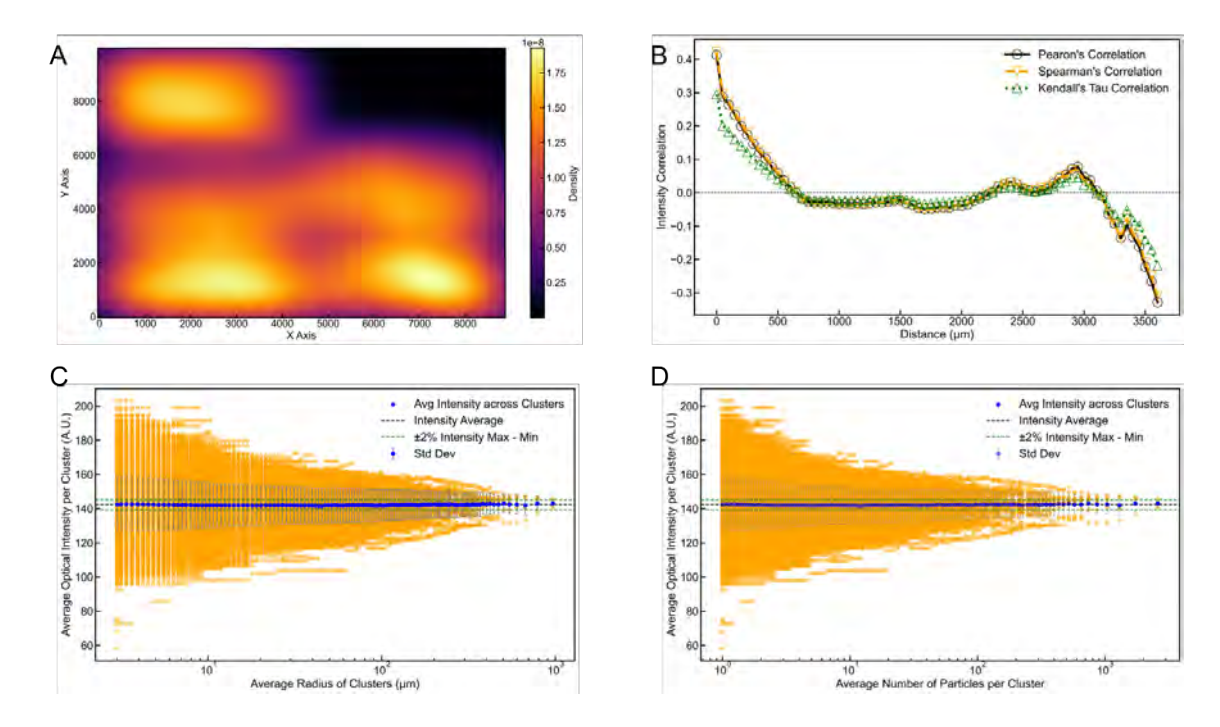


Fig. S38. Optical image analysis of NMC532 at SOC=100% during charging using 40X lens. (A) KDE heatmap of spatial data showing distribution of intensity-weighted datapoints across the coordinate space. Higher density regions (brighter color) correspond to clusters of high-intensity values. (B) Correlation analysis of the optical intensity of NMC particles as a function of spatial distance. Correlation coefficients are calculated within distance bins (width = $10~\mu m$ each) using three metrics: Pearson's, Spearman's, and Kendall's Tau. (C) Average optical intensity as a function of the increasing cluster size based on K-Means clustering of spatial coordinates of particle centroid. Blue points represent the mean intensity across clusters at a given spatial scale, and vertical error bars represent the standard deviation. Orange points show individual cluster intensities. Dashed horizontal lines represent global mean intensity (black) and $\pm 2\%$ thresholds (green) relative to the global intensity range. (D) The average optical intensity of NMC particles in a cluster as a function of the average number of particles per cluster. The average optical properties are not converged because of the poor quality of the optical image.

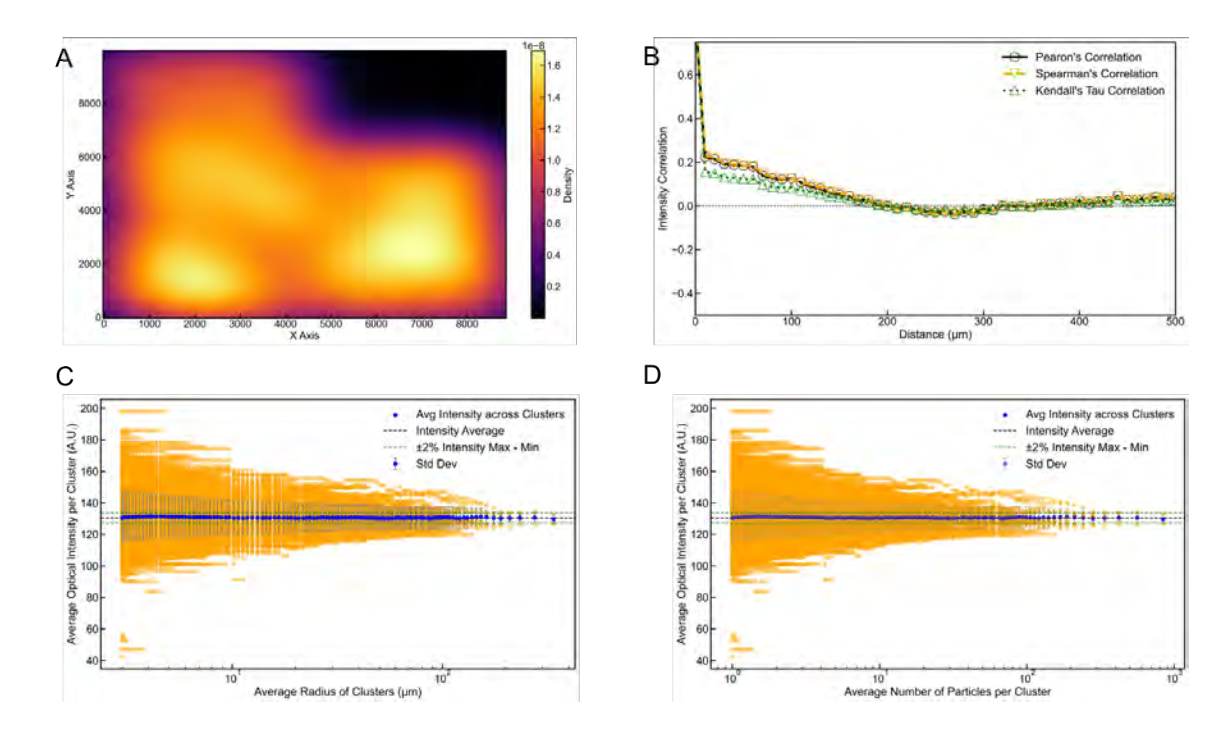


Fig. S39. Optical image analysis of NMC532 at SOC=100% during charging using 100X lens. (A) KDE heatmap of spatial data showing distribution of intensity-weighted datapoints across the coordinate space. Higher density regions (brighter color) correspond to clusters of high-intensity values. (B) Correlation analysis of the optical intensity of NMC particles as a function of spatial distance. Correlation coefficients are calculated within distance bins (width = 10 μ m each) using three metrics: Pearson's, Spearman's, and Kendall's Tau. (C) Average optical intensity as a function of the increasing cluster size based on K-Means clustering of spatial coordinates of particle centroid. Blue points represent the mean intensity across clusters at a given spatial scale, and vertical error bars represent the standard deviation. Orange points show individual cluster intensities. Dashed horizontal lines represent global mean intensity (black) and $\pm 2\%$ thresholds (green) relative to the global intensity range. (D) The average optical intensity of NMC particles in a cluster as a function of the average number of particles per cluster.

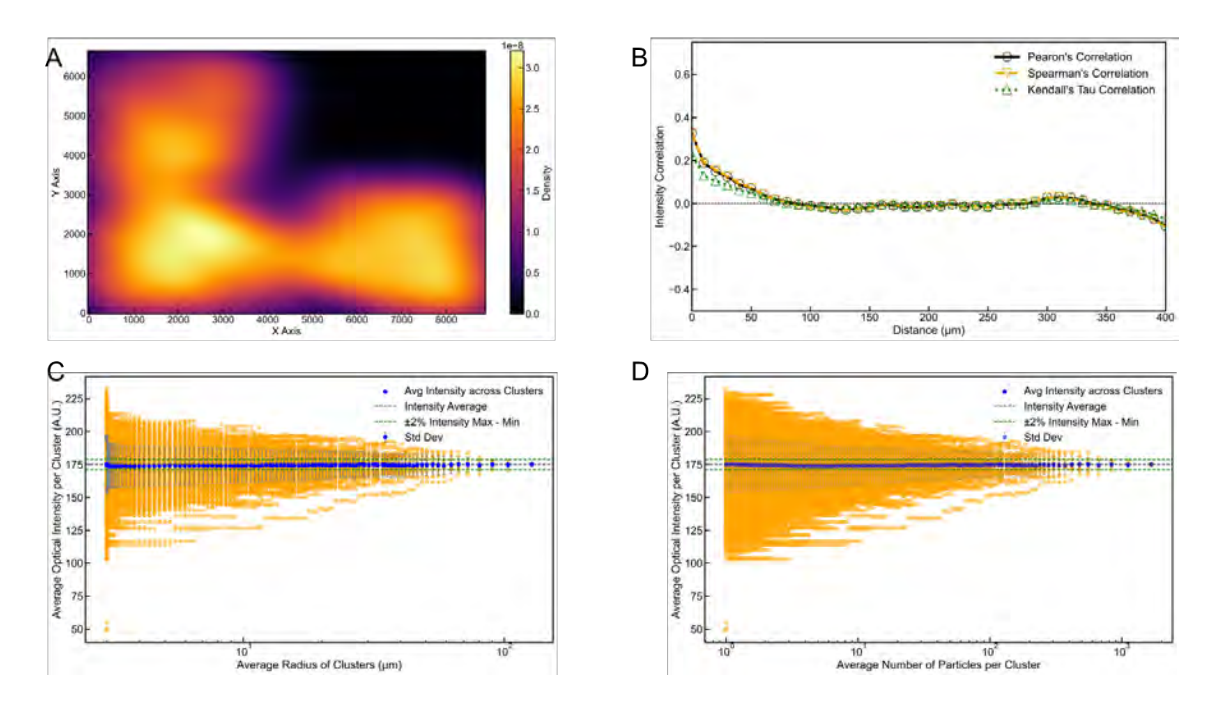


Fig. S40. Optical image analysis of NMC532 at SOC=100% (overcharged) during charging using 50X lens. (A) KDE heatmap of spatial data showing distribution of intensity-weighted datapoints across the coordinate space. Higher density regions (brighter color) correspond to clusters of high-intensity values. (B) Correlation analysis of the optical intensity of NMC particles as a function of spatial distance. Correlation coefficients are calculated within distance bins (width = $10~\mu m$ each) using three metrics: Pearson's, Spearman's, and Kendall's Tau. (C) Average optical intensity as a function of the increasing cluster size based on K-Means clustering of spatial coordinates of particle centroid. Blue points represent the mean intensity across clusters at a given spatial scale, and vertical error bars represent the standard deviation. Orange points show individual cluster intensities. Dashed horizontal lines represent global mean intensity (black) and $\pm 2\%$ thresholds (green) relative to the global intensity range. (D) The average optical intensity of NMC particles in a cluster as a function of the average number of particles per cluster.

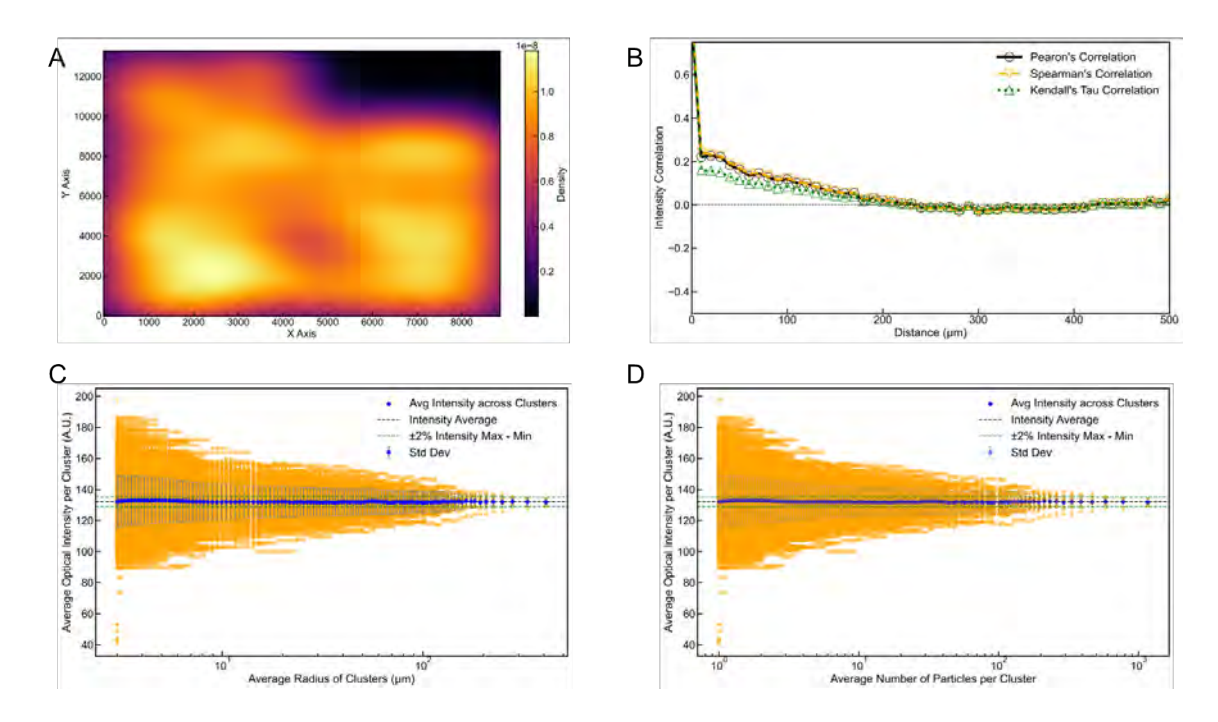


Fig. S41. Optical image analysis of NMC532 at SOC=100% (overcharged) during charging using 100X lens. (A) KDE heatmap of spatial data showing distribution of intensity-weighted datapoints across the coordinate space. Higher density regions (brighter color) correspond to clusters of high-intensity values. (B) Correlation analysis of the optical intensity of NMC particles as a function of spatial distance. Correlation coefficients are calculated within distance bins (width = $10~\mu m$ each) using three metrics: Pearson's, Spearman's, and Kendall's Tau. (C) Average optical intensity as a function of the increasing cluster size based on K-Means clustering of spatial coordinates of particle centroid. Blue points represent the mean intensity across clusters at a given spatial scale, and vertical error bars represent the standard deviation. Orange points show individual cluster intensities. Dashed horizontal lines represent global mean intensity (black) and $\pm 2\%$ thresholds (green) relative to the global intensity range. (D) The average optical intensity of NMC particles in a cluster as a function of the average number of particles per cluster.

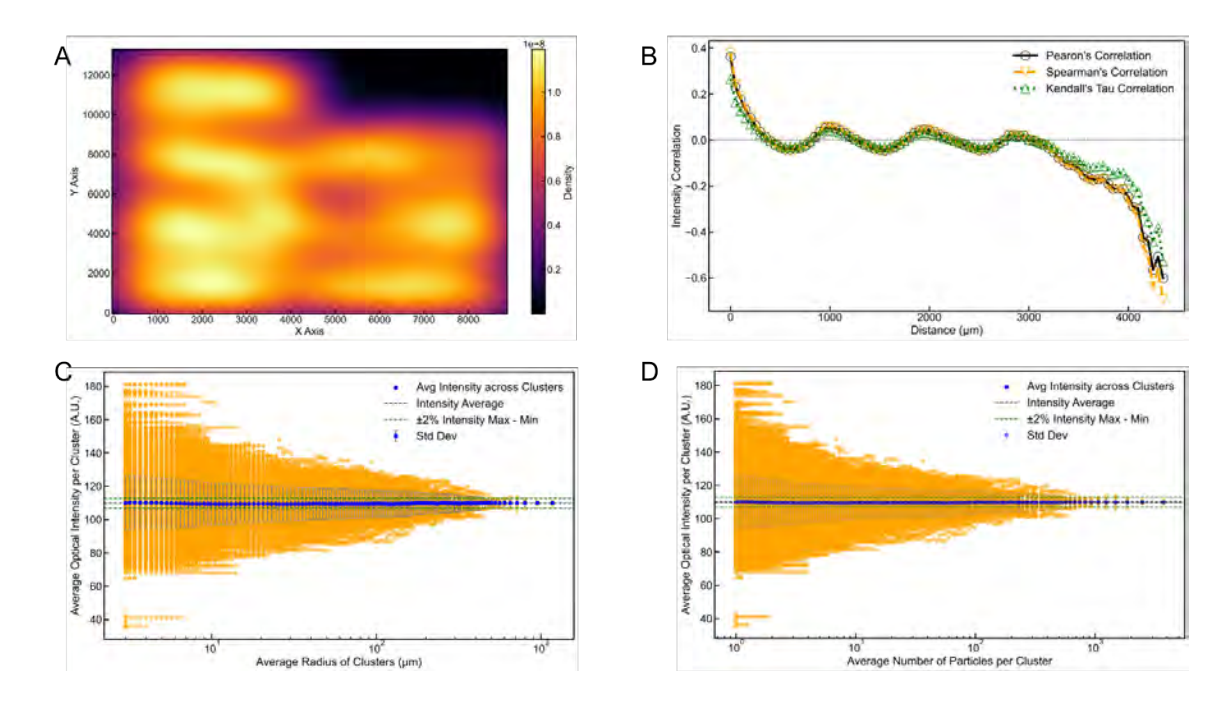


Fig. S42. Optical image analysis of NMC532 at SOC=72% during discharging using 40X lens. (A) KDE heatmap of spatial data showing distribution of intensity-weighted datapoints across the coordinate space. Higher density regions (brighter color) correspond to clusters of high-intensity values. (B) Correlation analysis of the optical intensity of NMC particles as a function of spatial distance. Correlation coefficients are calculated within distance bins (width = 10 μm each) using three metrics: Pearson's, Spearman's, and Kendall's Tau. (C) Average optical intensity as a function of the increasing cluster size based on K-Means clustering of spatial coordinates of particle centroid. Blue points represent the mean intensity across clusters at a given spatial scale, and vertical error bars represent the standard deviation. Orange points show individual cluster intensities. Dashed horizontal lines represent global mean intensity (black) and ±2% thresholds (green) relative to the global intensity range. (D) The average optical intensity of NMC particles in a cluster as a function of the average number of particles per cluster. The average optical properties are not converged because of the poor quality of the optical image. The average optical properties are not converged because of the poor quality of the optical image.

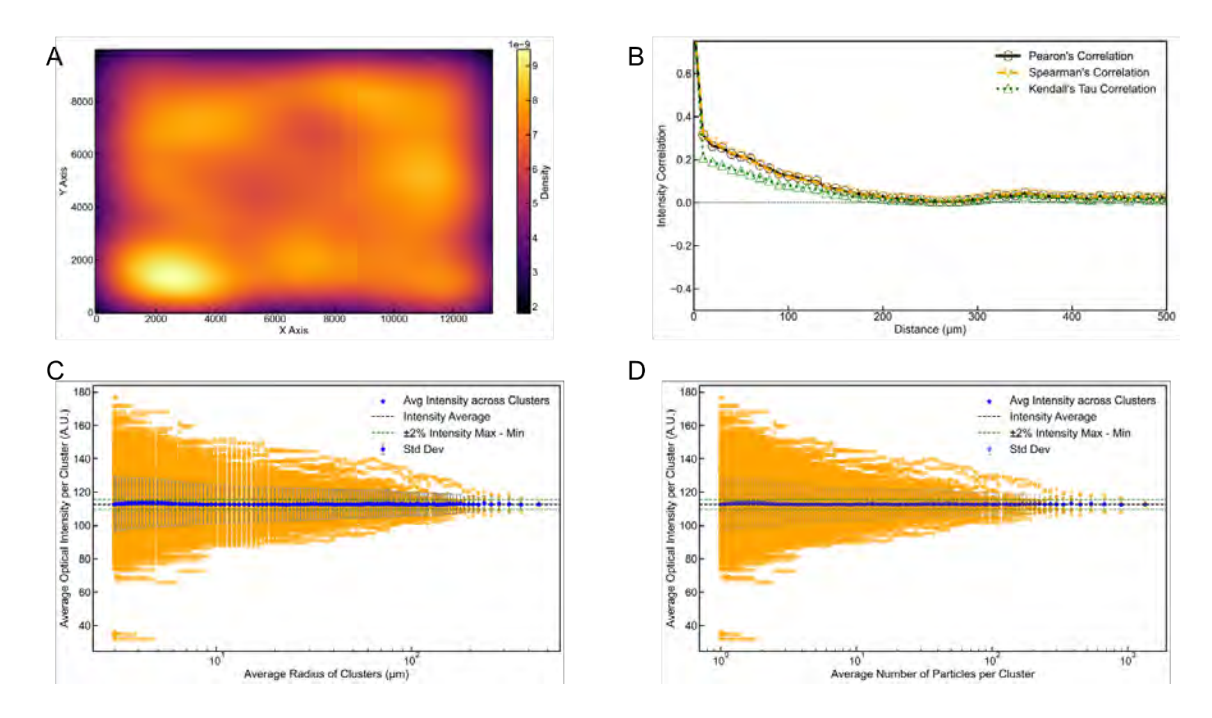


Fig. S43. Optical image analysis of NMC532 at SOC=72% during discharging using 100X lens. (A) KDE heatmap of spatial data showing distribution of intensity-weighted datapoints across the coordinate space. Higher density regions (brighter color) correspond to clusters of high-intensity values. (B) Correlation analysis of the optical intensity of NMC particles as a function of spatial distance. Correlation coefficients are calculated within distance bins (width = $10 \mu m$ each) using three metrics: Pearson's, Spearman's, and Kendall's Tau. (C) Average optical intensity as a function of the increasing cluster size based on K-Means clustering of spatial coordinates of particle centroid. Blue points represent the mean intensity across clusters at a given spatial scale, and vertical error bars represent the standard deviation. Orange points show individual cluster intensities. Dashed horizontal lines represent global mean intensity (black) and $\pm 2\%$ thresholds (green) relative to the global intensity range. (D) The average optical intensity of NMC particles in a cluster as a function of the average number of particles per cluster.

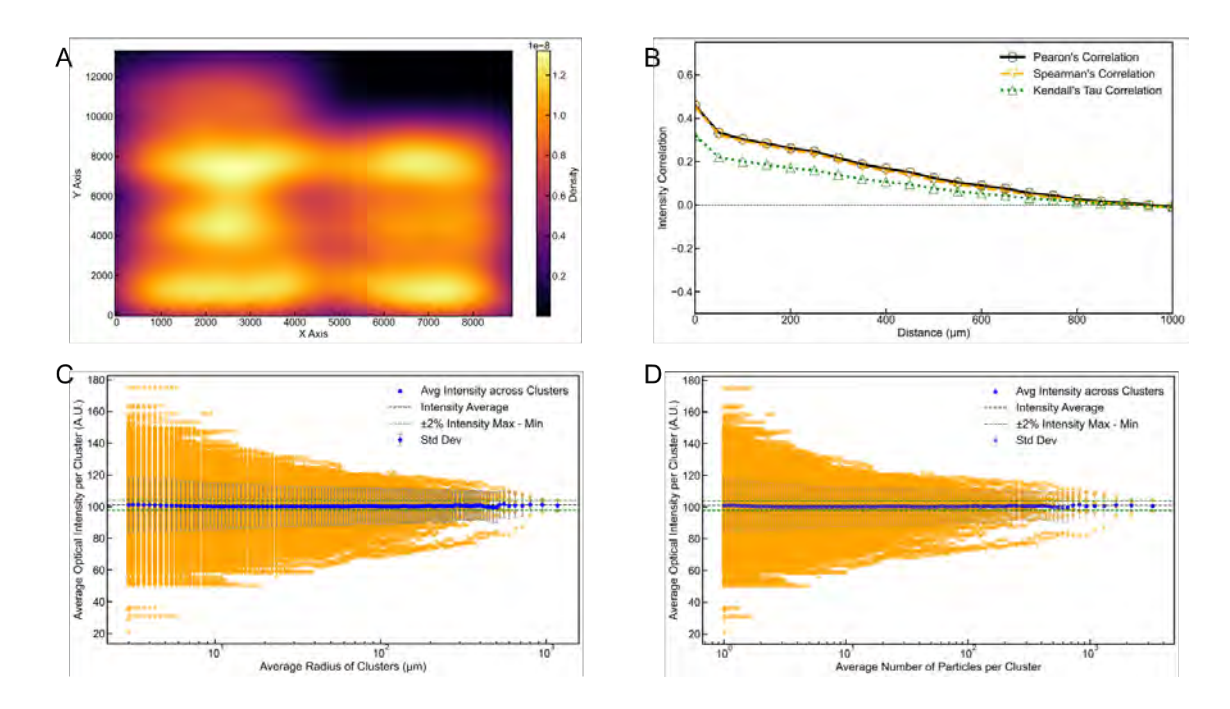


Fig. S44. Optical image analysis of NMC532 at SOC=65% during discharging using 40X lens. (A) KDE heatmap of spatial data showing distribution of intensity-weighted datapoints across the coordinate space. Higher density regions (brighter color) correspond to clusters of high-intensity values. (B) Correlation analysis of the optical intensity of NMC particles as a function of spatial distance. Correlation coefficients are calculated within distance bins (width = $10~\mu m$ each) using three metrics: Pearson's, Spearman's, and Kendall's Tau. (C) Average optical intensity as a function of the increasing cluster size based on K-Means clustering of spatial coordinates of particle centroid. Blue points represent the mean intensity across clusters at a given spatial scale, and vertical error bars represent the standard deviation. Orange points show individual cluster intensities. Dashed horizontal lines represent global mean intensity (black) and $\pm 2\%$ thresholds (green) relative to the global intensity range. (D) The average optical intensity of NMC particles in a cluster as a function of the average number of particles per cluster.

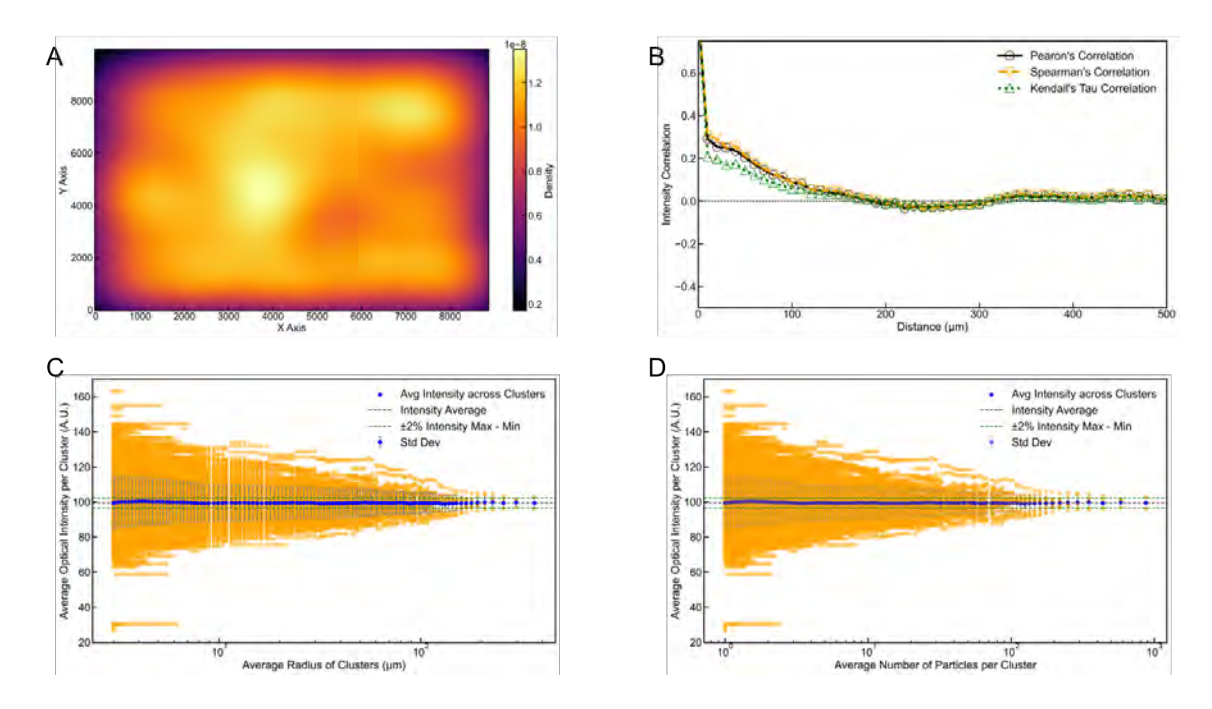


Fig. S45. Optical image analysis of NMC532 at SOC=65% during discharging using 100X lens. (A) KDE heatmap of spatial data showing distribution of intensity-weighted datapoints across the coordinate space. Higher density regions (brighter color) correspond to clusters of high-intensity values. (B) Correlation analysis of the optical intensity of NMC particles as a function of spatial distance. Correlation coefficients are calculated within distance bins (width = $10~\mu m$ each) using three metrics: Pearson's, Spearman's, and Kendall's Tau. (C) Average optical intensity as a function of the increasing cluster size based on K-Means clustering of spatial coordinates of particle centroid. Blue points represent the mean intensity across clusters at a given spatial scale, and vertical error bars represent the standard deviation. Orange points show individual cluster intensities. Dashed horizontal lines represent global mean intensity (black) and $\pm 2\%$ thresholds (green) relative to the global intensity range. (D) The average optical intensity of NMC particles in a cluster as a function of the average number of particles per cluster.

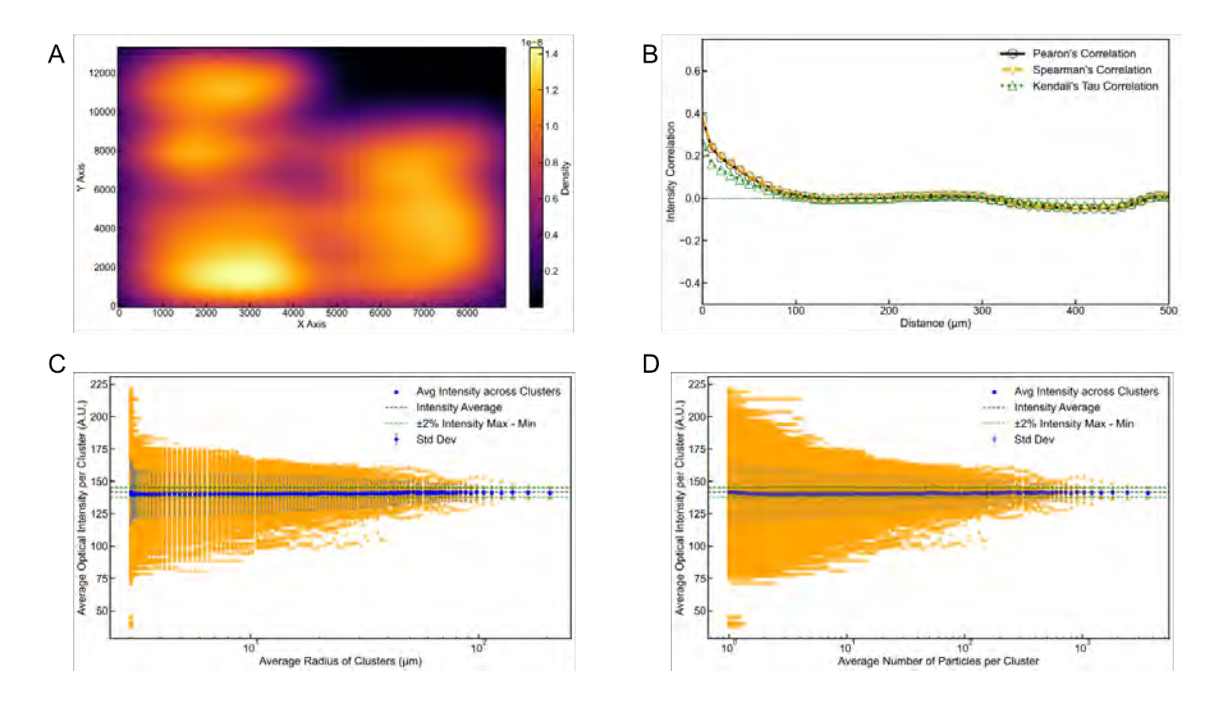


Fig. S46. Optical image analysis of NMC532 at SOC=57% during discharging using 50X lens. (A) KDE heatmap of spatial data showing distribution of intensity-weighted datapoints across the coordinate space. Higher density regions (brighter color) correspond to clusters of high-intensity values. (B) Correlation analysis of the optical intensity of NMC particles as a function of spatial distance. Correlation coefficients are calculated within distance bins (width = $10~\mu m$ each) using three metrics: Pearson's, Spearman's, and Kendall's Tau. (C) Average optical intensity as a function of the increasing cluster size based on K-Means clustering of spatial coordinates of particle centroid. Blue points represent the mean intensity across clusters at a given spatial scale, and vertical error bars represent the standard deviation. Orange points show individual cluster intensities. Dashed horizontal lines represent global mean intensity (black) and $\pm 2\%$ thresholds (green) relative to the global intensity range. (D) The average optical intensity of NMC particles in a cluster as a function of the average number of particles per cluster.

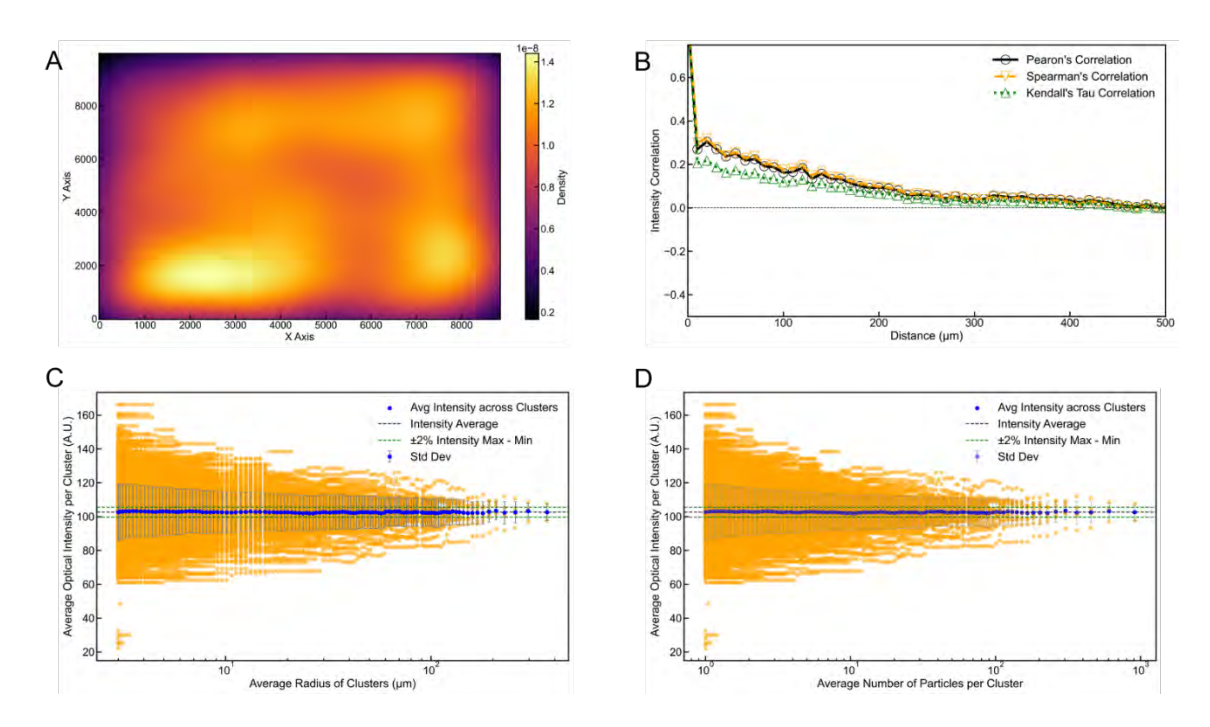


Fig. S47. Optical image analysis of NMC532 at SOC=57% during discharging using 100X lens. (A) KDE heatmap of spatial data showing distribution of intensity-weighted datapoints across the coordinate space. Higher density regions (brighter color) correspond to clusters of high-intensity values. (B) Correlation analysis of the optical intensity of NMC particles as a function of spatial distance. Correlation coefficients are calculated within distance bins (width = $10 \mu m$ each) using three metrics: Pearson's, Spearman's, and Kendall's Tau. (C) Average optical intensity as a function of the increasing cluster size based on K-Means clustering of spatial coordinates of particle centroid. Blue points represent the mean intensity across clusters at a given spatial scale, and vertical error bars represent the standard deviation. Orange points show individual cluster intensities. Dashed horizontal lines represent global mean intensity (black) and $\pm 2\%$ thresholds (green) relative to the global intensity range. (D) The average optical intensity of NMC particles in a cluster as a function of the average number of particles per cluster.

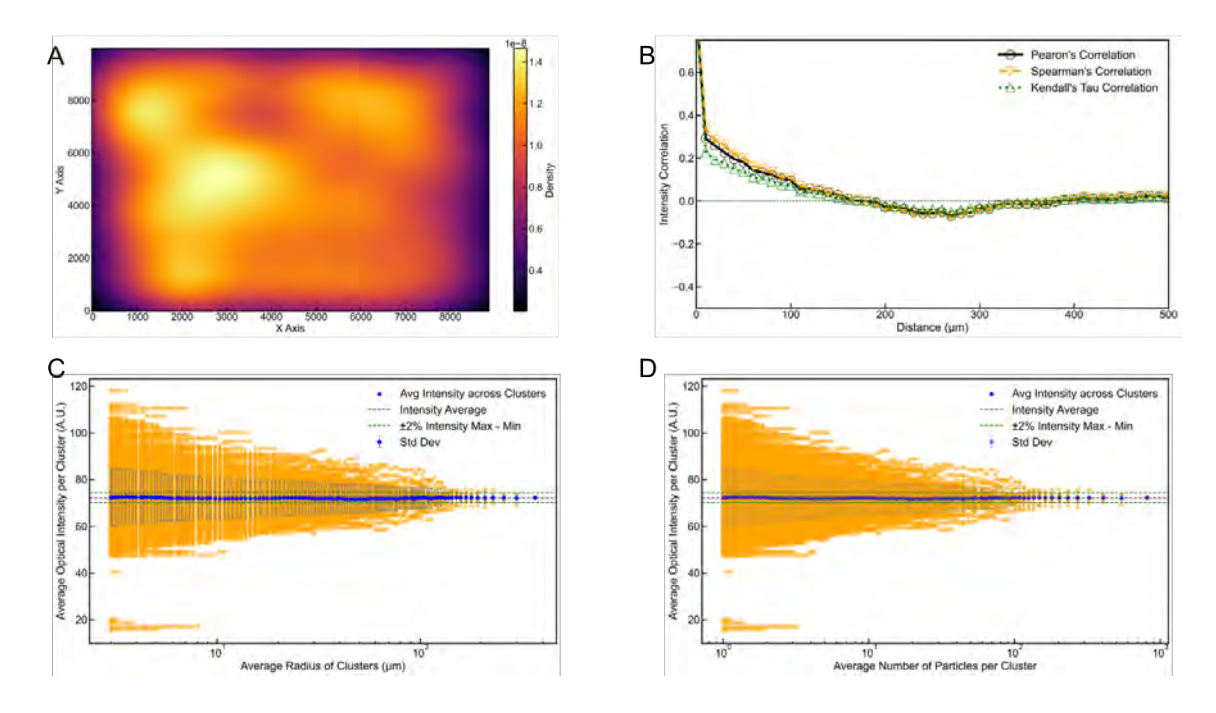


Fig. S48. Optical image analysis of NMC532 at SOC=40% during discharging using 100X lens. (A) KDE heatmap of spatial data showing distribution of intensity-weighted datapoints across the coordinate space. Higher density regions (brighter color) correspond to clusters of high-intensity values. (B) Correlation analysis of the optical intensity of NMC particles as a function of spatial distance. Correlation coefficients are calculated within distance bins (width = $10~\mu m$ each) using three metrics: Pearson's, Spearman's, and Kendall's Tau. (C) Average optical intensity as a function of the increasing cluster size based on K-Means clustering of spatial coordinates of particle centroid. Blue points represent the mean intensity across clusters at a given spatial scale, and vertical error bars represent the standard deviation. Orange points show individual cluster intensities. Dashed horizontal lines represent global mean intensity (black) and $\pm 2\%$ thresholds (green) relative to the global intensity range. (D) The average optical intensity of NMC particles in a cluster as a function of the average number of particles per cluster.

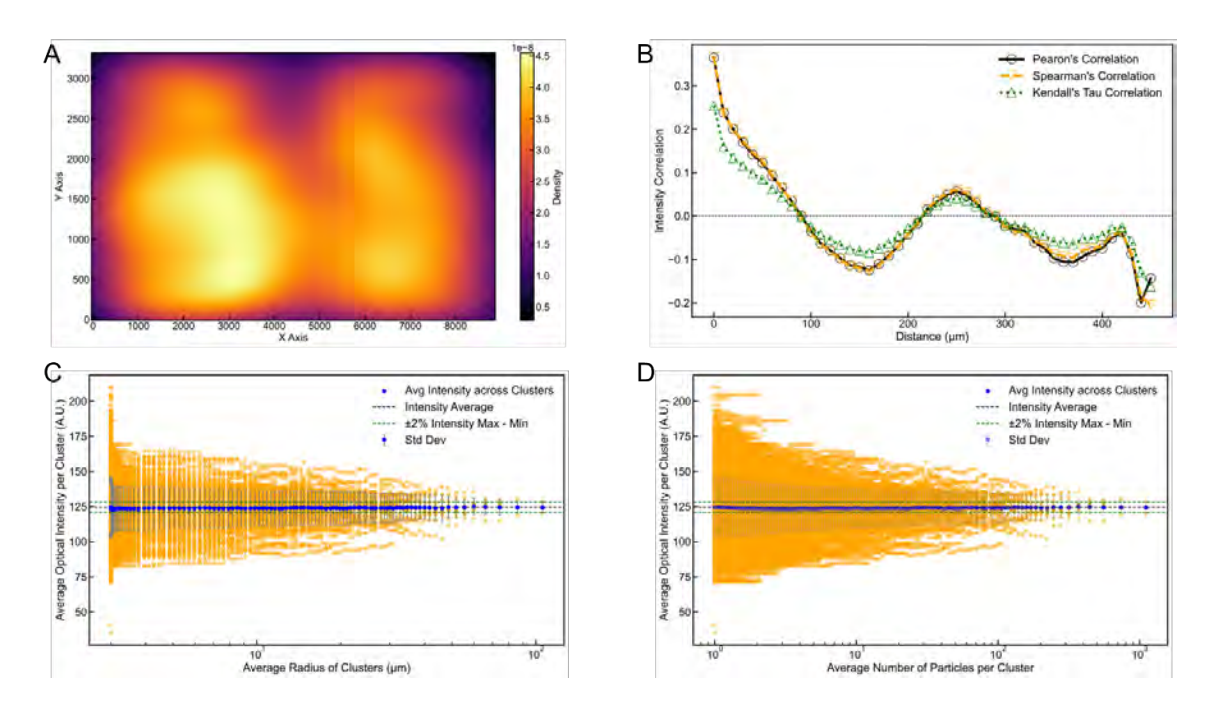


Fig. S49. Optical image analysis of NMC532 at SOC=30% during discharging using 50X lens. (A) KDE heatmap of spatial data showing distribution of intensity-weighted datapoints across the coordinate space. Higher density regions (brighter color) correspond to clusters of high-intensity values. (B) Correlation analysis of the optical intensity of NMC particles as a function of spatial distance. Correlation coefficients are calculated within distance bins (width = $10~\mu m$ each) using three metrics: Pearson's, Spearman's, and Kendall's Tau. (C) Average optical intensity as a function of the increasing cluster size based on K-Means clustering of spatial coordinates of particle centroid. Blue points represent the mean intensity across clusters at a given spatial scale, and vertical error bars represent the standard deviation. Orange points show individual cluster intensities. Dashed horizontal lines represent global mean intensity (black) and $\pm 2\%$ thresholds (green) relative to the global intensity range. (D) The average optical intensity of NMC particles in a cluster as a function of the average number of particles per cluster. The average optical properties are not converged because of the poor quality of the optical image.

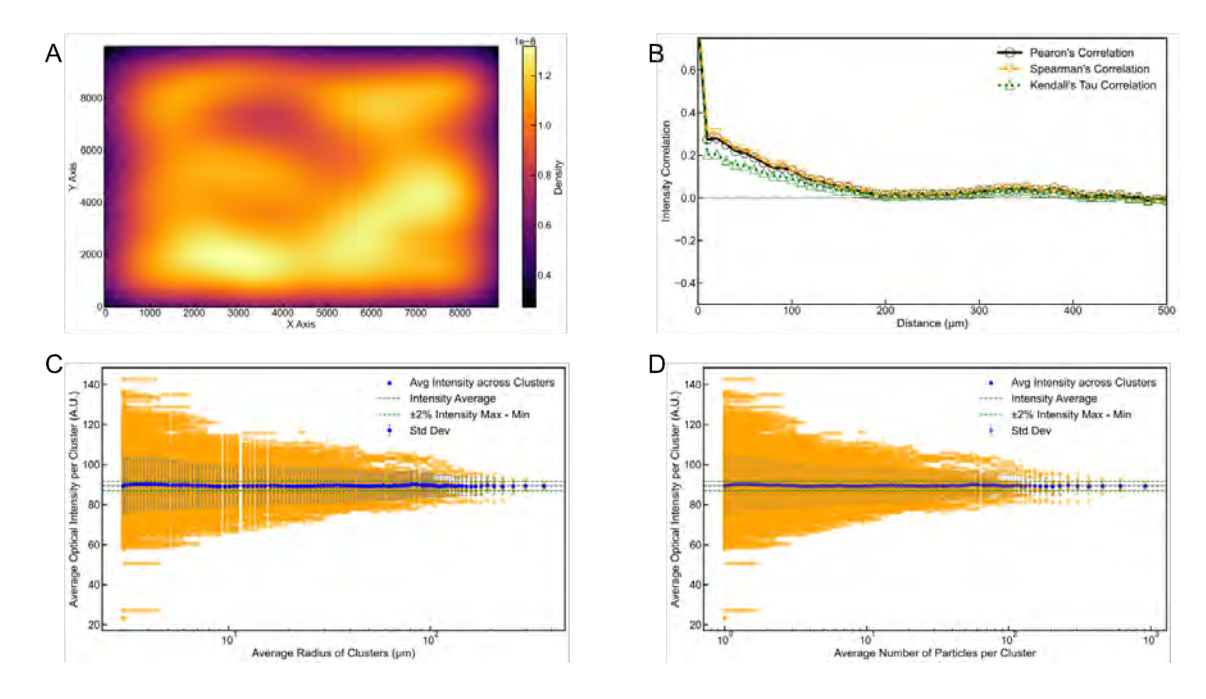


Fig. S50. Optical image analysis of NMC532 at SOC=30% during discharging using 100X lens. (A) KDE heatmap of spatial data showing distribution of intensity-weighted datapoints across the coordinate space. Higher density regions (brighter color) correspond to clusters of high-intensity values. (B) Correlation analysis of the optical intensity of NMC particles as a function of spatial distance. Correlation coefficients are calculated within distance bins (width = $10~\mu m$ each) using three metrics: Pearson's, Spearman's, and Kendall's Tau. (C) Average optical intensity as a function of the increasing cluster size based on K-Means clustering of spatial coordinates of particle centroid. Blue points represent the mean intensity across clusters at a given spatial scale, and vertical error bars represent the standard deviation. Orange points show individual cluster intensities. Dashed horizontal lines represent global mean intensity (black) and $\pm 2\%$ thresholds (green) relative to the global intensity range. (D) The average optical intensity of NMC particles in a cluster as a function of the average number of particles per cluster.

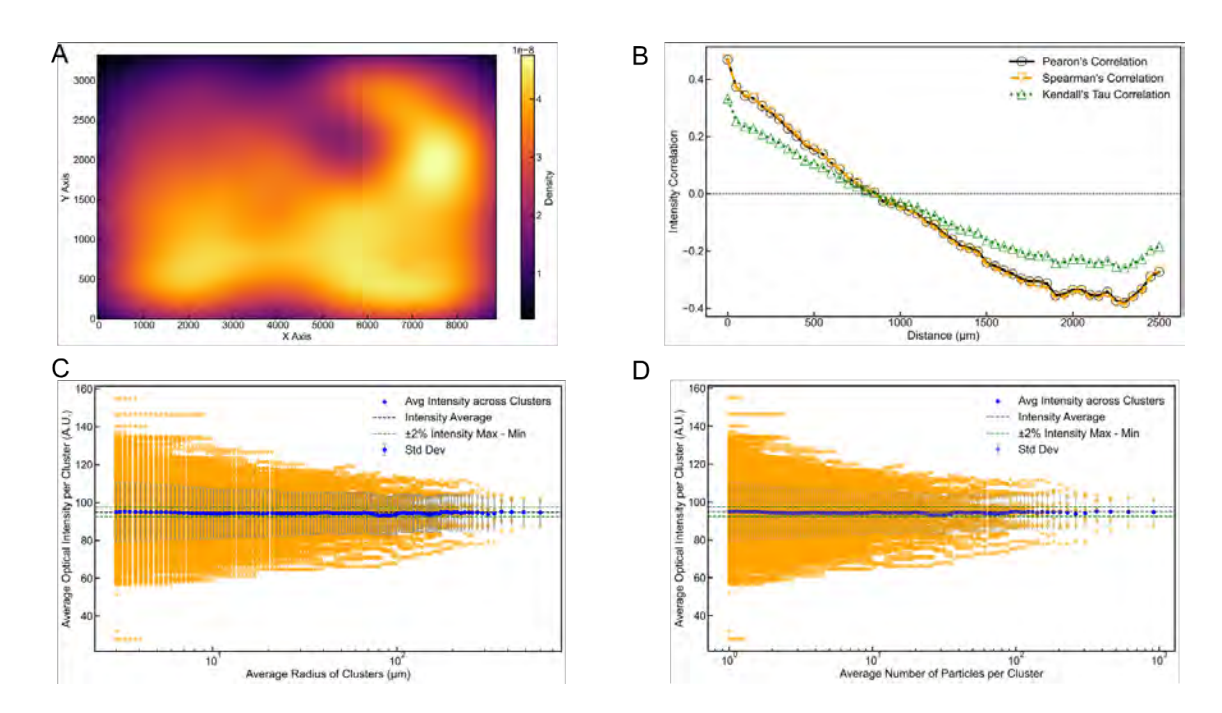


Fig. S51. Optical image analysis of NMC532 at SOC=8% during discharging using 40X lens. (A) KDE heatmap of spatial data showing distribution of intensity-weighted datapoints across the coordinate space. Higher density regions (brighter color) correspond to clusters of high-intensity values. (B) Correlation analysis of the optical intensity of NMC particles as a function of spatial distance. Correlation coefficients are calculated within distance bins (width = $10~\mu m$ each) using three metrics: Pearson's, Spearman's, and Kendall's Tau. (C) Average optical intensity as a function of the increasing cluster size based on K-Means clustering of spatial coordinates of particle centroid. Blue points represent the mean intensity across clusters at a given spatial scale, and vertical error bars represent the standard deviation. Orange points show individual cluster intensities. Dashed horizontal lines represent global mean intensity (black) and $\pm 2\%$ thresholds (green) relative to the global intensity range. (D) The average optical intensity of NMC particles in a cluster as a function of the average number of particles per cluster. The average optical properties are not converged because of the poor quality of the optical image.

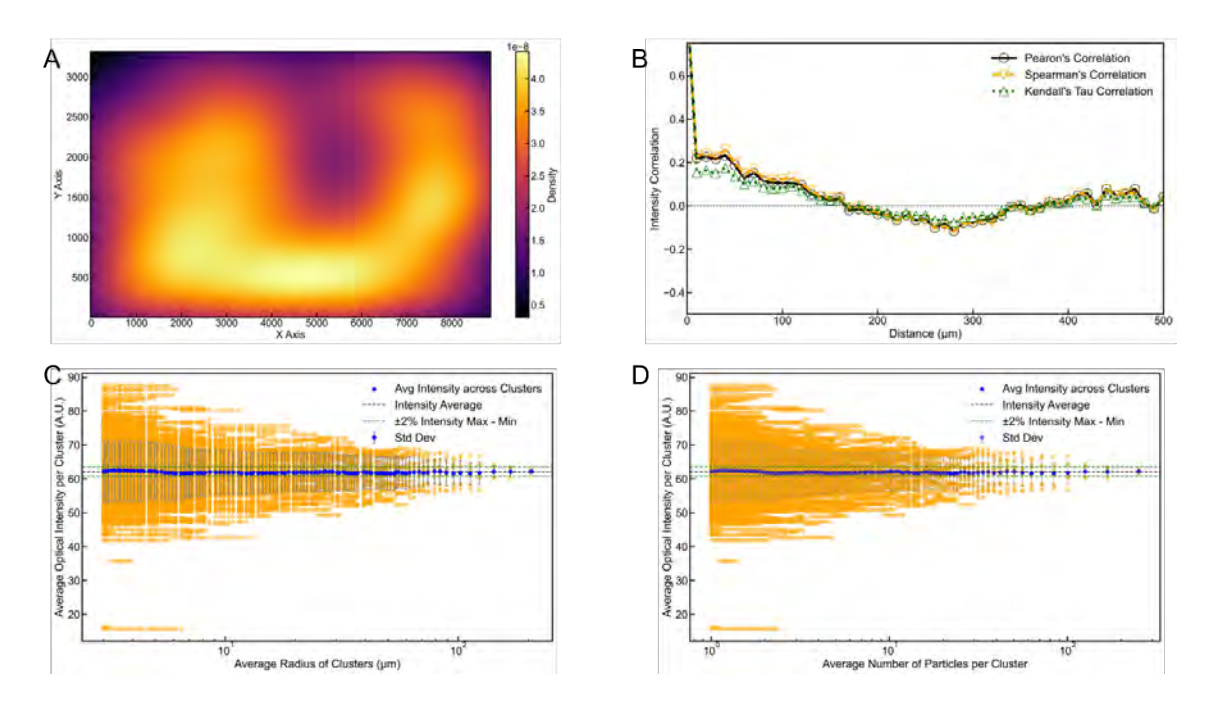


Fig. S52. Optical image analysis of NMC532 at SOC=8% during discharging using 100X lens. (A) KDE heatmap of spatial data showing distribution of intensity-weighted datapoints across the coordinate space. Higher density regions (brighter color) correspond to clusters of high-intensity values. (B) Correlation analysis of the optical intensity of NMC particles as a function of spatial distance. Correlation coefficients are calculated within distance bins (width = 10 μ m each) using three metrics: Pearson's, Spearman's, and Kendall's Tau. (C) Average optical intensity as a function of the increasing cluster size based on K-Means clustering of spatial coordinates of particle centroid. Blue points represent the mean intensity across clusters at a given spatial scale, and vertical error bars represent the standard deviation. Orange points show individual cluster intensities. Dashed horizontal lines represent global mean intensity (black) and $\pm 2\%$ thresholds (green) relative to the global intensity range. (D) The average optical intensity of NMC particles in a cluster as a function of the average number of particles per cluster.

Movie S1. Animation of Li distribution in the NMC composite electrode at different SOCs calculated by finite element modeling. The particles are color coded according to the Li composition. The color bar represents x in Li_{1-x}(NMC)O₂.

SI References

- 1. L. D. a. L. Landau, E.M., *Quantum Mechanics: Non-relativistic Theory* (Butterworth-Heinemann, London, ed. 3rd, 1976).
- 2. H. Weng, Y. Kawazoe, X. Wan, J. Dong, Electronic structure and optical properties of layered perovskites Sr 2 MO 4 (M= Ti, V, Cr, and Mn): an ab initio study. *Physical Review B—Condensed Matter and Materials Physics* **74**, 205112 (2006).
- 3. C. Ambrosch-Draxl, J. O. Sofo, Linear optical properties of solids within the full-potential linearized augmented planewave method. *Computer physics communications* **175**, 1-14 (2006).
- 4. B. Adolph, J. Furthmüller, F. Bechstedt, Optical properties of semiconductors using projector-augmented waves. *Physical Review B* **63**, 125108 (2001).
- 5. M. Gajdoš, K. Hummer, G. Kresse, J. Furthmüller, F. Bechstedt, Linear optical properties in the projector-augmented wave methodology. *Physical Review B—Condensed Matter and Materials Physics* **73**, 045112 (2006).
- 6. D. R. Penn, Wave-number-dependent dielectric function of semiconductors. *Physical review* **128**, 2093 (1962).
- 7. R. Amin, Y.-M. Chiang, Characterization of electronic and ionic transport in Li1-xNi0. 33Mn0. 33Co0. 33O2 (NMC333) and Li1-xNi0. 50Mn0. 20Co0. 30O2 (NMC523) as a function of Li content. *Journal of The Electrochemical Society* **163**, A1512 (2016).
- 8. H.-J. Noh, S. Youn, C. S. Yoon, Y.-K. Sun, Comparison of the structural and electrochemical properties of layered Li [NixCoyMnz] O2 (x= 1/3, 0.5, 0.6, 0.7, 0.8 and 0.85) cathode material for lithium-ion batteries. *Journal of power sources* **233**, 121-130 (2013).
- 9. M. Dixit, B. Markovsky, F. Schipper, D. Aurbach, D. T. Major, Origin of structural degradation during cycling and low thermal stability of Ni-rich layered transition metal-based electrode materials. *The journal of physical chemistry C* **121**, 22628-22636 (2017).
- 10. H. Sun, K. Zhao, Electronic structure and comparative properties of LiNi x Mn y Co z O2 cathode materials. *The Journal of Physical Chemistry C* **121**, 6002-6010 (2017).
- 11. N. Sharma, L. S. d. Vasconcelos, S. Hassan, K. Zhao, Asynchronous-to-synchronous transition of Li reactions in solid-solution cathodes. *Nano Letters* **22**, 5883-5890 (2022).
- 12. A. Shrivastava, N. Sharma, X. He, Y. Liu, K. Zhao. Scale of Heterogeneity data files [Data set]. *Zenodo* (2025). doi: 10.5281/zenodo.15870101.